



Review

Active Brazing for Energy Devices Sealing

Jian Feng ^{*}, Marion Herrmann, Anne-Maria Reinecke and Antonio Hurtado

Chair of Hydrogen Technology and Nuclear Power Engineering, Dresden University of Technology (TUD),
George-Bähr-Str. 3, D-01062 Dresden, Germany

* Correspondence: jian.feng@tu-dresden.de; Tel.: +49-(351)-463-34904

Abstract: The pursuit of reliable energy devices sealing solutions stands as a paramount engineering challenge for ensuring energy safety and dependability. This review focuses on an examination of recent scientific publications, primarily within the last decade, with a central aim to grasp and apply critical concepts relevant to the efficient design and specification of brazements for ceramic–metal active-brazed assemblies, emphasizing the sealing of energy devices. The goal is to establish robust and enduring joints capable of withstanding water-vapor and hydrogen environments. The review commences with a concise recapitulation of the fundamental principles of active brazing, followed by an in-depth exploration of material selection, illustrated using water-vapor-resistant sensors as illustrative examples. Furthermore, the review presents practical solutions for the sealing of energy devices while also scrutinizing the factors that exert significant influence on the deterioration of these active-brazed connections. Ultimately, the review culminates in a comprehensive discussion of emerging trends and developments in active brazing techniques for energy-related applications.

Keywords: active brazing; energy; laser



Citation: Feng, J.; Herrmann, M.; Reinecke, A.-M.; Hurtado, A. Active Brazing for Energy Devices Sealing. *J. Exp. Theor. Anal.* **2024**, *2*, 1–27. <https://doi.org/10.3390/jeta2010001>

Academic Editor: Marco Rossi

Received: 20 November 2023

Revised: 20 December 2023

Accepted: 29 December 2023

Published: 12 January 2024



Copyright: © 2024 by the authors. Licensee MDPI, Basel, Switzerland. This article is an open access article distributed under the terms and conditions of the Creative Commons Attribution (CC BY) license (<https://creativecommons.org/licenses/by/4.0/>).

1. Introduction

Germany has firmly positioned itself as an early investor and a driving force in shaping climate policy, making significant strides towards achieving climate neutrality. The nation has set an ambitious target of attaining climate neutrality by 2045, necessitating the phased-out use of fossil fuels from its energy mix, accelerated adoption of renewable energies, and a focused effort to reduce overall energy consumption [1]. Notably, securing the supply of energy is just as important as the energy transition itself. Consequently, the development of robust energy sensor encapsulation and reactor sealing solutions has become a challenging engineering task in ensuring energy safety and reliability.

Addressing the distinct packaging requirements of each sensor/reactor device is essential to ensure their optimal performance when interacting with external devices or the surrounding environment. The following review focuses on the application of active brazing for energy devices sealing, with a primary emphasis on energy reactors or storage sensors that play a crucial role in energy safety.

Of particular interest for these applications are the high demands for signal transmission and local electrical isolation, which have sparked considerable attention towards the bonding of ceramic–ceramic and ceramic–metal joints. However, joining advanced ceramics, even with each other, presents a non-trivial challenge due to their strong ionic or covalent bonding and the low self-diffusivity of constituent atoms or ions, making solid-state bonding difficult. Moreover, the task of bonding ceramics to metals is even more complex for two reasons [2,3]. First, there is a disparity in chemical bonding between the covalent or ionic advanced ceramics and the metallic metals to which they are joined. Second, there is a mismatch in the coefficient of thermal expansion (CTE) between these materials, with ceramics generally having significantly lower CTEs than metals. Consequently, high-stress concentrations can occur, and generally, interlayers are employed to maintain the gradual transition of material properties at the joints.

Despite the aforementioned obstacles, various liquid-phase joining techniques have been developed for bonding ceramics to both themselves and metals. Figure 1 demonstrates the temperature capability of these liquid-phase joining techniques, offering potential solutions to the intricate challenge of joining dissimilar materials in energy devices sealing. Among these solutions, brazing stands out due to its distinctive characteristics. It involves working at temperatures exceeding 450 °C but still below the melting point of the materials to be joined. This method allows the creation of ceramic–ceramic and ceramic–metal joints through two different approaches: indirect brazing, where ceramic surfaces are first metallized and then brazed using conventional filler metals, and direct (active) brazing, which utilizes filler alloys containing active elements like titanium [2–6] or metal oxides like CuO [7–9]. Brazing offers several significant advantages. It is particularly well suited for joining dissimilar materials or components with distinct properties. Furthermore, brazing proves to be highly adaptable for mass production, making it an efficient choice in industrial settings.

Reviews [2,5,10] have effectively established the fundamentals of active brazing. The pros and cons of diverse techniques for metal-to-ceramic joining are detailed [11–13], and discussions on microstructure and heat transfer in specific systems can be found in [14–16]. Previous research has primarily concentrated on furnace processes, particularly in the context of energy device sealing for solid oxide fuel cells (SOFCs) [17,18]. However, there is a noticeable gap in the literature, with a limited focus on application areas and a lack of an overarching and systematic exploration of energy device sealing.

The main focus of this review is to delve into specific research papers, particularly from scientific journals published within the last decade. The primary objective is to comprehend and apply the concepts essential for effectively designing and specifying brazements for ceramic–metal active-brazed assemblies, with a particular emphasis on energy devices sealing. This involves creating robust, durable joints suitable for water-vapor and hydrogen environments. In the subsequent sections of the review, the fundamental principles of active brazing are briefly reiterated. Following that, there is a detailed explanation of materials selection, using laser active brazing of water-vapor resistant sensors as exemplars. Additionally, the review provides viable solutions for sensor devices sealing. The careful consideration of the evidence presented identifies the key factors that have significant impact on the degradation of the brazed joints. Finally, the review concludes with a thorough discussion of emerging areas in active brazing techniques for energy applications.

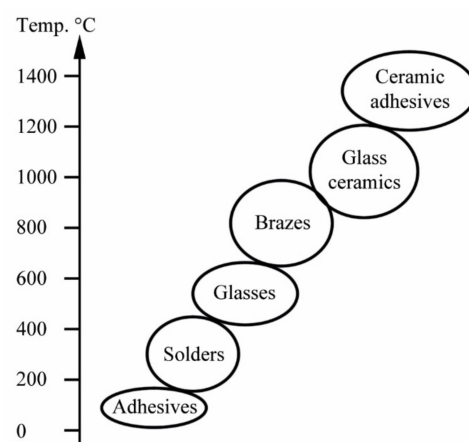


Figure 1. Temperature-resistance characteristics of different liquid-phase joining methods, categorized according to Fernie and Hanson [19].

2. Fundamentals of Active Brazing

Lately, active brazing has been garnering increasing attention within the brazing community. This growing interest can be attributed to the excellent wetting properties of active brazing alloys (ABAs) with most ceramic materials. As depicted in Figure 2,

active brazing offers a unique joining approach that allows for the use of standard brazing techniques when creating metal–ceramic brazements, eliminating the need for ceramic substrate metallization, as typically required in conventional brazing processes [20].

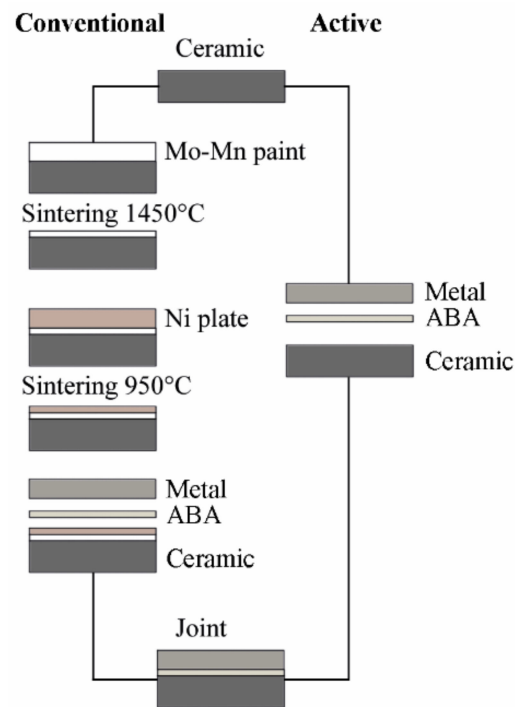


Figure 2. Comparison of conventional and active brazing techniques.

Active brazing technology can be categorized into two primary groups: active metal brazing and active oxide brazing. The former, often referred to simply as active brazing, is the more widely recognized method. The feature of active metal brazing lies in the utilization of stable oxide, carbide, or nitride formers such as titanium (as shown in Tables 1–3), zirconium (see references from Sandia National Laboratories [21]), or hafnium [22]. These elements play a crucial role in the active metal-brazing process. While other active elements like chromium, vanadium, and molybdenum have been successfully employed in ABAs, the most commercially successful ones belong to group IVB elements. The interconnection at interfaces is achieved by a drastic redox reaction [23], and only small amounts of the active element within the ABA are necessary for hermetic, strongly bonded joints. During active metal brazing, spreading and flow (capillary flow) of the ABA is highly limited by the bare oxide ceramic surface. High-vacuum or inert atmospheres are required for most active brazing processes because excessive oxygen in the atmosphere can react with the active element in ABA and compromise its efficiency. Very thin layers of ABA, e.g., several hundreds of microns, are generally used in the most applications.

If the composition of the filler metals of active metal brazing can be carefully adjusted, it becomes possible to regulate the oxidation process of the susceptible components. In other words, the oxidation products should be evenly distributed within the filler metals and resistant to transformation and coarsening. This requirement leads to another class of active brazing known as active oxide brazing or the more common reactive air brazing (RAB). For instance, by reducing the copper content in a commercial ABA like CB4 ((Ag_{27.3}Cu)₉₇Ti₃) from its Ag–Cu eutectic concentration of approximately 27.3% to 8% and subsequently subjecting it to oxidation in the ambient air, the Ag–Cu–Ti active metal-brazing system transforms into an Ag–CuO–TiO₂ reactive air-brazing system.

The RAB method is notably gentler in comparison to active metal brazing (AMB). Incorporating a pre-oxidation stage serves to boost both the resistance to oxidation and the wettability of the filler substances on ceramic surfaces. This process of interconnection at

interfaces relies on the exchange of oxygen and/or vacancies. Consequently, the formation of pores (type II in Figure 3) is inherent to RAB and cannot be entirely avoided [24,25]. To address this, the introduction of a small quantity of aluminum into the brazing mixture has proven effective in pore reduction [24]. However, it is important to avoid an excessively high fraction of oxide at the interfaces, as this can lead to the amplification of complex brittle phases and potential initiation of cracks [26].

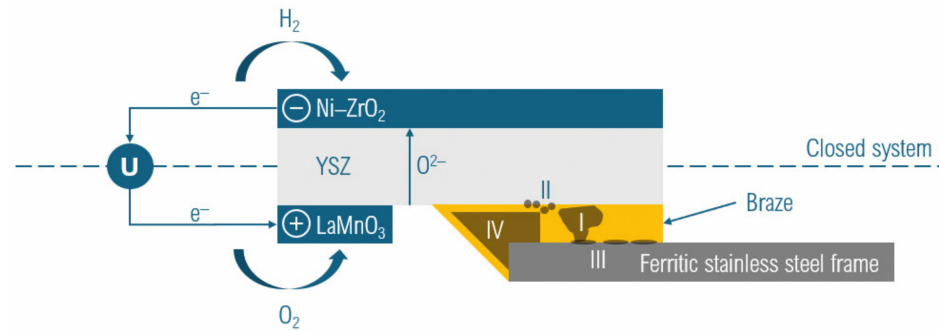


Figure 3. Schematic of a standard planar solid oxide fuel cell (SOFC) supported by a stainless steel picture frame. Various pore types are illustrated as follows: Type I pores result from brazing faults, type II represents interfacial pores formed during the reduction of CuO, type III showcases a porous structure at stainless-steel-braze interfaces induced by thermal cycles, and type IV denotes gaseous water pockets formed from the recombination of hydrogen and oxygen that has migrated into the braze.

The primary technological advantage of active brazing lies in its streamlined, one-step process [2]. This eliminates the need for the multi-step metallization typically involved, and most ABAs are readily available in the market. However, active brazing demands more stringent tolerance in brazed assemblies, and it is limited in terms of joint geometries.

Active brazing is characterized by a relatively narrow process window influenced by multiple variables that must be strictly followed. The heating times and rates must be meticulously maintained, and the narrow temperature range for the brazing reactions must be carefully observed. Failure to adhere to the required parameters can affect the quality of the brazed seam. To achieve optimum results in active brazing, careful and precise execution is required.

3. Brazement Materials Selection for Water-Vapor Resistant Sensors

3.1. Background

Hydrothermal energy sensors that are faster, more accurate, and more compact in comparison to existing solutions require leak-tight signal feedthroughs, which demand ceramic-to-metal seals with excellent insulation, outgassing, and leak-tightness properties [27,28]. Thin-film metallization is currently the leading technology for performing ceramic-to-metal seals [11,21]. The deposition of ultra-thin, high-quality metal films with improved properties and performance is still the ongoing goal of many developers though it is complex, costly, and time-consuming. Alternatively, joining ceramics to metals is becoming more efficient with active brazing and laser-assisted techniques, hereinafter referred as laser active brazing. Laser active brazing offers considerable economic benefits over traditional deposition methods in that the joining can be established in a single-step operation with localized heat input realized within several seconds. Automated laser active brazing is highly focused and minimizes thermal input by selective heating and improves the performance and reliability of the components.

For hydrothermal multiphase flow imaging, the current generation of wire-mesh sensors commonly used for hydrothermal multiphase flow imaging still relies on polymers like PEEK (polyether ether ketone) and PTFE (polytetrafluoroethylene) as the sealants to ensure hermeticity, and this limits the application temperature of these sensors to below

300 °C [29]. Designing the wire-mesh sensors for temperatures up to 400 °C and maximum pressures of 150 bar would significantly expand the possible applications.

An outline of materials selection for laser-brazed signal feedthroughs of miniaturized energy sensors is, however, still missing. Indeed, performing the most suitable materials selection for a specific application is an intrinsic part of scientific design and innovation [30] and requires careful consideration. In the present work, materials selection is carried out for signal feedthroughs of miniaturized energy sensors with the aim of manufacturing reliable joints by laser brazing. These brazed joints should be hermetic, withstand high temperatures and pressures, and connect the electrodes to insulators. At the same time, the joints should be highly ductile in order to minimize the probability of failure due to thermally induced stress. The miniaturized energy sensors, generally including needle probes and signal feedthroughs of grid sensors, can be subsequently plugged into the sensor body, as shown in Figure 4. The distance between two adjacent sensors is approximately 3 mm.

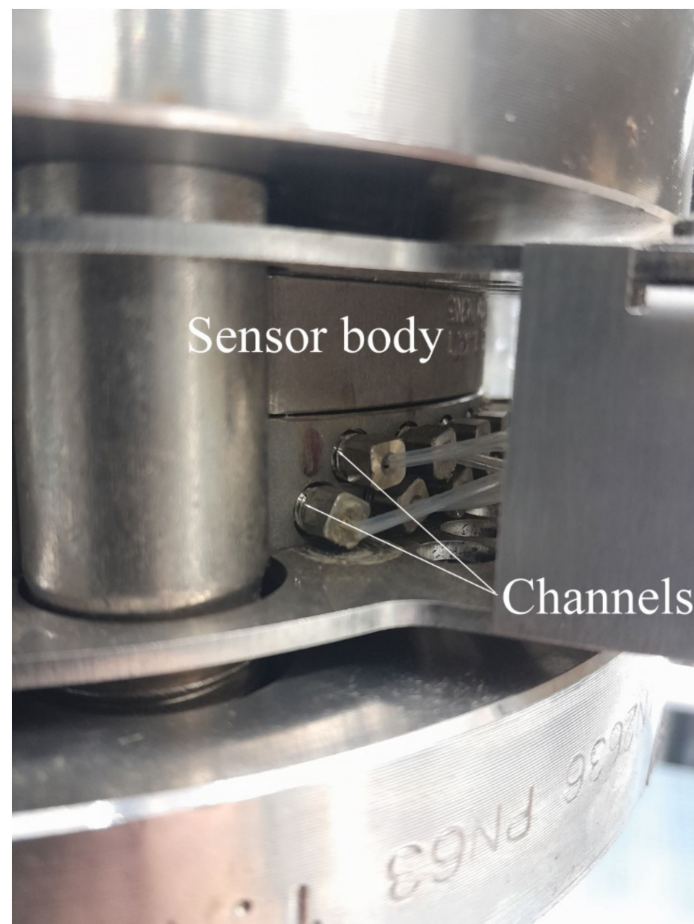


Figure 4. Channels, each with a diameter of 3 mm, are incorporated into a grid sensor specifically designed to accommodate signal feedthroughs tailored for the SECA device. This sensor is allocated within our facilities.

3.2. Multiple Attribute Decision-Making (MADM) Process

The MADM is used in the present work to select the materials that ensure a high functionality of needle probes and signal feedthroughs [31]. This method can perform the solution procedure regardless of the functional relationship between the objectives and constraints. The number of attributes (rating criteria) and alternatives (potential materials) applicable to the process is computationally limitless. The present MADM process consists

of an entropy weighting step to determine the weights of attributes and a step of technique for order preference by similarity to ideal solution (TOPSIS) to rank all the alternatives.

For weights calculations, the entropy of x_{ij} , i.e., the j th index of the i th alternative, is determined by the following:

$$H_j = -\frac{\sum_{i=1}^m f_{ij} \ln f_{ij}}{\ln m}, j = 1, 2, \dots, n, \tag{1}$$

wherein

$$f_{ij} = \frac{r_{ij}}{\sum_{i=1}^m r_{ij}}, j = 1, 2, \dots, n.$$

Here, r_{ij} is the rescaled value of x_{ij} . Then, the sensibility or the entropy weight of x_{ij} is determined by the following:

$$w_j = \frac{1 - H_j}{n - \sum_{j=1}^n H_j}, \tag{2}$$

with

$$\sum_{j=1}^n w_j = 1.$$

TOPSIS is used as a solution method. To calculate the normalized decision matrix V ,

$$V = \left[\frac{x_{ij}}{\sqrt{\sum_{i=1}^m x_{ij}^2}} \right]_{m \times n}, j = 1, 2, \dots, n. \tag{3}$$

To determine the positive/negative ideal solutions from V ,

$$\left\{ \begin{aligned} \{V_1^+, V_2^+, \dots, V_n^+\} &= \left\{ \max_i V_{ij} | j \in J, \min_i V_{ij} | j \in J', i = 1, 2, \dots, m \right\} \\ \{V_1^-, V_2^-, \dots, V_n^-\} &= \left\{ \min_i V_{ij} | j \in J, \max_i V_{ij} | j \in J', i = 1, 2, \dots, m \right\} \end{aligned} \right.$$

To calculate the n -dimensional Euclidean distances,

$$\left\{ \begin{aligned} d_i^+ &= \sqrt{\sum_{j=1}^n w_j (V_{ij} - V_j^+)^2}, i = 1, 2, \dots, m \\ d_i^- &= \sqrt{\sum_{j=1}^n w_j (V_{ij} - V_j^-)^2}, i = 1, 2, \dots, m \end{aligned} \right. \tag{4}$$

The relative closeness of alternatives to the ideal solution is then given by the following:

$$Cl_i^+ = \frac{d_i^-}{d_i^+ + d_i^-}; i = 1, 2, \dots, m. \tag{5}$$

Alternatives with higher magnitudes of closeness that are closer to 1 are preferred.

3.3. Attributes and Alternatives

The proper selection of attributes (rating criteria) and alternatives (laser-machinable materials) are key points in an MADM process. During a decision path, criteria are selected with superior performance while maintaining minimal interactions between them.

Table 1 presents the primary attributes considered for the three material categories (metal, ceramic, and ABAs), including CTE and Young’s modulus. These properties play a significant role in determining the maximum theoretical thermal residual stress occurring during the laser active brazing process. Additionally, the shear modulus, flexural strength, and fracture toughness are taken into account to evaluate the width of the process window for laser active brazing. In this regard, ceramics with higher values of these parameters may

have a better chance of surviving during brazing. The water-vapor resistance of alternatives is assessed based on the weight loss rate of ceramics in hydrothermal atmospheres at elevated temperatures [32–34]. This weight loss can be attributed to the volatilization reactions of water vapor that occur in oxidizing atmospheres.

When selecting metallic interconnects for energy sensors, two crucial attributes to consider are resistance against hydrogen embrittlement and corrosion resistance in various water media. The mechanical properties of alloys are tested both before and after hydrogen exposure at ambient temperature [35], and alloys that exhibit higher yield strength and lower ductility after hydrogen exposure are deemed more prone to hydrogen embrittlement. However, all the chosen alternatives (alloys) demonstrate similar high corrosion resistance in different water qualities, resulting in low sensitivity by weighting these attributes.

One of the main challenges in implementing feedthroughs for miniaturized energy sensors is finding suitable sealants that provide both hermeticity and hydrothermal resistance. In this context, a soft active sealant with a relatively low brazing temperature and thermophysical properties similar to ceramics is generally preferred. While the thermal conductivity of active sealants is a crucial consideration in addressing high-temperature capillarity and gapping problems, unfortunately, no information is available on the hydrothermal resistance of the sealants, so this parameter could not be used as the main characteristic. In the event that the joint is not hydrothermally resistant, an additional corrosion protection layer must be applied.

3.4. Selected Materials

By using the data listed in Table 1 and calculating from the MADM process, the relative closeness in percentages was used to grade each alternative. As shown in Figure 5, the stable oxides of elements from the IV main group were selected as the most appropriate ceramic materials for the brazement, followed by the commonly used material alumina. Austenitic stainless steels were chosen as the most appropriate metallic interconnects. Ag-based active alloys distinguish themselves for the brazement due mainly to their “soft” nature.

Despite the advantages of laser-assisted methods, the successful brazing of materials using lasers requires optimization of the brazement design to minimize thermal residual stress. Among the various material combinations, joining austenitic stainless steels/Ag–Cu–Ti/alumina can be particularly challenging due to the large mismatches in the coefficients of thermal expansion and Young’s modulus, which lead to extreme stress concentrations. Consequently, laser active brazing has not yet been widely used for these material combinations, although some preliminary attempts have been made, and valuable experience has been gained. Meanwhile, the high demand for these materials has led to a large number of studies using furnace processes. Table 2 presents the strength of brazed alumina-to-metal joints reported in the literature, where Ag-based active brazing alloys were employed in all cases. The most extensively studied system is the alumina/304 combination, which has exhibited an average joint strength below 100 MPa regardless of the type of testing. To reduce thermal stress, small joint geometries are preferred. In summary, it seems that furnace processes have reached their limits, and it would be interesting to investigate if the limits could be overcome by laser active brazing.

The performance of an ABA can often be limited by its oxidation properties when exposed to high operating temperatures. Thus, the oxidation resistance of Ag-based ABAs, especially the Ag–Cu–Ti system, needs to be addressed. This system has been studied as gas seals for solid oxide fuel cells, and its application limit in air is approximately 600–700 °C [36,37]. The oxidation of Ag–Cu–Ti filler metals is primarily governed by copper oxidation, and no oxides of titanium and silver are formed if the amount of Ti remains small. Ag–Cu brazes have been widely used for cladding steam turbine blades without direct exposure to steam and have been qualified for engine service on many assemblies up to 426.7 °C (800 °F) [38]. However, their application at higher temperatures in steam is limited by gas dissolution and their diffusion in Ag. To solve this problem, co-alloying Al or coating at brazement may be considered in future work. Adding Al to the

Ag–Cu–Ti system has been shown to improve oxidation resistance by forming an adherent protective CuAl_2O_4 film without sacrificing its excellent wettability [39]. Alternatively, coating technologies for gas turbines can be directly transferred to current applications.

The use of MADM processes can be extremely beneficial when dealing with engineering decision problems that require the representation of objectives and constraints through numerical data. This study focuses on the materials selection process for laser-brazed signal feedthroughs of miniaturized energy sensors. The MADM process involved evaluating each component separately to identify the most proper water-vapor-resistant ceramics, metallic interconnects, and active sealants. The entropy and TOPSIS methods were utilized, demonstrating satisfactory results in both weighting and obtaining a solution.

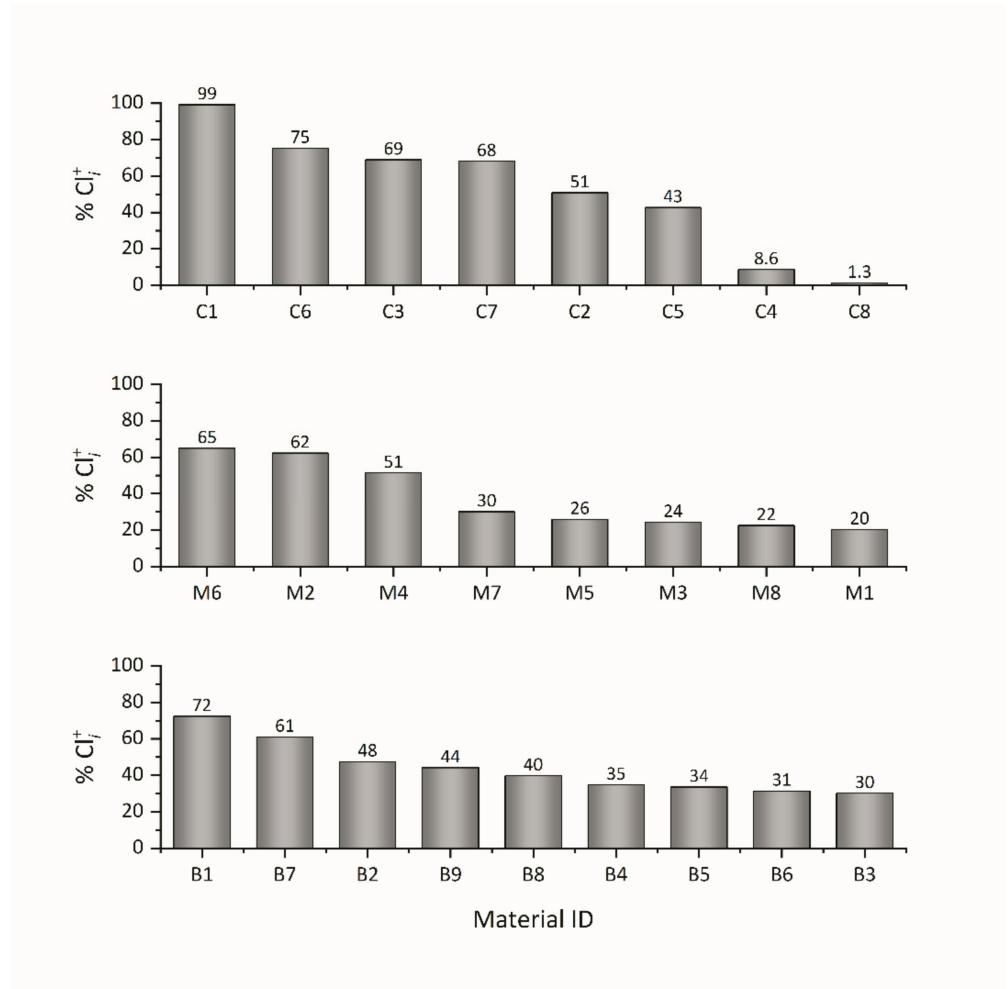


Figure 5. Results of materials selection using MADM process.

Table 1. Suggested materials for signal feedthroughs of miniaturized energy sensors. All elastic constants and mechanical properties were determined at 20 °C.

		CTE 20–500 °C (ppm/K)	Young’s Modulus (GPa)	Shear Modulus (GPa)	Flexural Strength (MPa)	Fracture Toughness (MPa√m)	Weight Loss Rate ^a (μg/cm ² h)												
C1	ZrO ₂ (98%, 1.9% HfO ₂ , stabilized)	11.7	210	81	1050	6.5	0												
C2	Yb ₂ SiO ₅	6.3	149	61	215	2.3	1												
C3	Y ₂ SiO ₅	8.3	123	47	100	2.2	3												
C4	Al ₂ TiO ₅	1.6	16	96	40	4.0	9												
C5	Mullite	5.4	151	55	180	2.0	11												
C6	TiO ₂	9.0	228	89	137	3.2	22												
C7	Al ₂ O ₃ (99.6%)	8.2	390	159	470	4.0	23												
C8	SiO ₂ (99.99%, fused)	0.7	72	31	104	1.1	100												
								Ratio ^b Yield Strength	Ratio ^b UTS	Ratio ^b Reduction in Area	Ratio ^b Elongation	Uniform Corr.	Pitting/ Crevice	Erosion	Sulfide Attack	SICC ^c	Impingement	Water Quality ^d	Cost ^e
								-	-	-	-	-	-	-	-	-	-	-	-
M1	304	18	200	1.11	0.89	0.41	0.65	1	2	1	1	1	1	1	1	1	F	6	
M2	316Ti	19	200	1.00	1.06	0.99	1.06	1	2	1	1	1	1	1	1	1	F	6.5	
M3	318LN	15	200	0.97	0.89	0.46	0.63	1	2	1	1	1	1	1	1	1	F	10	
M4	Titanium G2	9.7	107	1.03	0.82	0.56	0.60	1	1	1	1	1	1	1	1	1	F/B/S	36	
M5	Sea-Cure	11	217	1.05	0.89	0.50	0.55	1	1	1	1	1	1	1	1	1	F/B/S	11	
M6	AL-6X	16	195	1.02	0.97	1.02	1.02	1	1	1	1	1	1	1	1	1	F/B/S	17	
M7	AL-29-4C	10.8	207	1.09	0.81	0.55	0.58	1	1	1	1	1	1	1	1	1	F/B/S	12	
M8	Inconel 718	14.4	170	0.99	0.91	0.32	0.45	2	2	1	4	2	2	2	2	2	F/B/S	100	
								Liquidus Temp. (°C)	Solidus Temp. (°C)	Yield Strength (MPa)	UTS (MPa)								
B1	CB2	22	71	970	970	60	130												
B2	CB4	19	80	805	780	230	271												
B3	Ticuil	19	85	900	780	292	339												
B4	Cusil-ABA	19	83	815	780	271	346												
B5	Cusin-1 ABA	19	83	806	775	260	402												
B6	Incusil-ABA	18	76	715	605	338	455												
B7	Silver-ABA	21	77	912	860	136	282												
B8	Gold-ABA	16	87	1030	1003	209	334												
B9	Au-4Ti	14	82	1064	1063	195	310												

Notes: ^a at approx. 1500 °C, 1 bar, and steam flow of 100 m/s; ^b ratio of test results after and before hydrogen exposure; ^c SICC = strain-induced corrosion cracking; ^d F = fresh water, B = brackish water, S = sea water; ^e data from the Indian market in the year 2019 to 2022. CTE means coefficients of thermal expansion; UTS means ultimate tensile strength; Corr. means corrosion; Temp. means temperature.

Table 2. Reported strength of brazed alumina–metal joints using active braze alloys (ABA).

ABA	Composition	Melting Range (°C)	Metal	Strength (MPa)	Test Type	Geometry	Braze Thickness (µm)	Brazing Temp. (°C)	Brazing Duration (ks)	Atm.	Atm. Pressure (Pa)	Laser Power (W)	Ref.
Cusil–ABA	Ag35.25Cu1.75Ti	780–815	304	88 ± 8	Shear	Rectangular lap	50	830	0.6	HV	1 × 10 ^{−5}		[40]
Cusin-1 ABA	(Ag35Cu) ₉₇ Ti ₂ Sn ₁	775–806	304	89.8 ± 4	Shear	Double lap	30–40	800–850	0.6	HV			[41]
Cusin-1 ABA	(Ag35Cu) ₉₇ Ti ₂ Sn ₁	775–806	304	21.9 ± 0.6	Tensile	Disc/bar tee	30–40	800–850	0.6	HV			[41]
m-BAg-8	(Ag28Cu) _{100-x} Ti _x		304	63	Tensile	Tubular butt	100	900	0.6	HV	1 × 10 ^{−3}		[42]
m-BAg-8	(Ag28Cu) ₉₄ Ti ₆ -W		304	13.2	Tensile	Single lap	50	900	1.8	HV	3 × 10 ^{−4}		[43]
Cusil–ABA	Ag35.25Cu1.75Ti	780–815	304	13.5	Tensile	Single lap	50	900	1.8	HV	3 × 10 ^{−4}		[43]
CB4	(Ag27.3Cu) ₉₇ Ti ₃	780–805	304			Rectangular lap	100			Ar		144	[44]
Zrcusil	Ag1Cu2Zr		304L	114	Tensile	ASTM F19		985	0.3	UHV			[21]
m-BAg-8	(Ag28Cu) ₉₇ Ti ₃	780–805	321	18.4	Shear	Disc butt	50	850	0.6	HV	5 × 10 ^{−3}		[45]
Ticusil	(Ag28Cu) _{95.5} Ti _{4.5}	780–900	630	170	Shear	Rectangular lap	100	880	0.6	HV	6 × 10 ^{−3}		[46]
Incusil–ABA	Ag27.2Cu12.5In1.25Ti	605–715	A108	42	Shear	Tubular butt	200	950	0.12–0.18	Ar		320	[47]
CB4	(Ag27.3Cu) ₉₇ Ti ₃	780–805	100Cr6/C45E	82	Bending	Butt	50			Ar		300–360	[48]
Cusil–ABA	Ag35.25Cu1.75Ti	780–815	Kovar	97	Tensile	ASTM F19		825	0.12	Ar			[21]
m-BAg-8	(Ag28Cu) ₉₂ Ti ₈		Kovar	78	Tensile	ASTM F19		890	0.3	HV	3 × 10 ^{−3}		[49]
Cusil–ABA	Ag35.25Cu1.75Ti	780–815	Kovar	60 ± 15	Tensile	ASTM F19	50	844	0.12	V	4 × 10 ^{−1}		[50]
Ticusil	(Ag28Cu) _{95.5} Ti _{4.5}	780–900	Kovar	67 ± 4	Shear	Rectangular lap	100	850	0.6	HV	1 × 10 ^{−3}		[51]
Cusil–ABA (outdated)	(Ag28Cu) ₉₈ Ti ₂		Kovar	29 ± 13	Shear	Rectangular lap	100	840	0.6	HV	7 × 10 ^{−2}		[52]
m-BAg-8	(Ag28Cu) ₉₈ (TiH ₂) ₂		TiAl	102	Shear	Rectangular lap	100–150	880	0.6	HV	3 × 10 ^{−4}		[53]

Notes: Temp. means temperature; Atm. means atmosphere; Ref. means references; V means vacuum; HV means high vacuum; UHV means ultra-high vacuum.

Table 3. Reported data of brazed alumina–metal joints using active braze alloys (ABA) for SOEC/SOFC applications.

ABA	Ceramic	Metal	RT Strength (MPa)	Test Type	Geometry	Braze Thickness (μm)	Brazing Temp. ($^{\circ}\text{C}$)	Brazing Duration (ks)	Atm.	Atm. Pressure (Pa)	Load (MPa)	Ref.
Ticusil	3YSZ	Ferritic SS	40 ± 8	Shear	Rectangular lap	100–120	915	0.3	HV	1×10^{-4}		[54]
Ticusil	8YSZ	1.4755			Rectangular lap	50	900	0.6	HV	5×10^{-3}		[55]
Ag0.5Al	3YSZ											
Ag8Cu	8YSZ	1.4760			Rectangular lap		970–1150	1.2	Air			[56]
Ag8Cu0.5Ti	Al_2O_3											
Ag0.5Al		1.4755										
Ag4Cu	3YSZ	(Crofer22H)			Rectangular lap	100	1000	0.6	Air		1.5	[9]
Ag8Cu												
Ag28Cu + TiH_2	3YSZ	1.4301 (304)	$< \sim 90$	Shear	Disc/bar		820–860	0.6–3	HV	7×10^{-3}		[57]
Ag4CuO	Al_2O_3 (99.6%)	1.4760 (Crofer22APU)	$\leq 115 \pm 10$	Shear	Rectangular lap	76	1000–1100	0.3	Air			[58]
Ag8CuO	8YSZ	1.4760	≤ 21.3 at 550°C	Shear	Rectangular butt	100			Air			[59]
Ag4CuO	3YSZ	Aluminized 1.4755	≤ 44.3		Rectangular lap	~ 200	950–1100	1.8	Air			[60]
Ag2CuO	CGO	Aluminized 1.4755	39 ± 3	Shear	Rectangular butt	100	1000	1.2	Air		0.1	[61]
Ag8CuO	YSZ	Coated 1.4760	55 ± 3	Shear	Rectangular lap	~ 150	1050	1.8	Air		1×10^{-3}	[62]
Ag $_x$ CuO	YSZ	1.4016 (430)			Disc/bar	~ 700	950	1.8	Air			[63]
Ag–CuO– TiO_2	LSCoF	Fecralloy					950–1100	1.8	Air			[64]
Ag $_x$ CuAlO $_2$	3YSZ	1.4845 (310S)							Air		4.7×10^{-3}	[65]
Ag $_x$ Al $_2$ TiO $_5$	YSZ	1.4760			Rectangular lap	~ 29	920–950	1.2	Air			[66]
Ticusil– Al $_2$ TiO $_5$ / TiH_2	8YSZ	1.4016				< 500	880	0.3				[36]
Ag $_x$ V $_2$ O $_5$	LSCoF		26 ± 9	Bending	Rectangular butt		1000/1100	1.8	Air			[67]
Ag $_5$ Nb $_2$ O $_5$	YSZ	1.4845 (310S)	< 110	Shear	Rectangular lap	< 250	1150	1.8	Air			[68]
Ag $_x$ SiO $_2$	8YSZ		≤ 47	Shear	Rectangular lap		1050	1.8	Air		2	[69]

Notes: RT means room temperature; Temp. means temperature; Atm. means atmosphere; Ref. means references.

4. Solutions to Energy Devices Sealing

The performance metrics of commercial sensors and reactors can differ among manufacturers, and the encapsulation/sealing technologies they use can also vary. Each encapsulation/sealing technique exhibits distinctive analytical patterns as well as its own set of benefits and drawbacks. Familiarity with these patterns simplifies the process of optimizing sensor encapsulation and reactor sealing for their intended uses.

4.1. Nuclear Reactors

Within the realm of nuclear energy generation, encompassing both fusion and fission processes, the demands placed on joints are exceptionally rigorous. The materials utilized for joining must be well suited to a neutron-rich environment [70], and the joining methodologies need to align with the design principles of the nuclear reactors. This entails the reliable and practical joining of ceramic components, which can extend several meters in length yet remain only a few millimeters thick. Notably, the utilization of pressure-free techniques is a possibility. Among the various composite materials, options such as carbon fiber composites (CFCs) and silicon carbide fiber-reinforced composites (SiC_f/SiC) have emerged as candidates for deployment in distinct nuclear settings encompassing both fusion and fission scenarios.

Initially, CFCs were earmarked for use as plasma-facing materials within a crucial component of the ITER project—the divertor [71,72]. Despite the fact that CFCs have now been replaced by tungsten (W) in the final ITER design, significant engineering headway has been made in countering their pronounced erosion and substantial tritium absorption within redeposited layers [73]. The amalgamation of CFCs with metallic materials can be readily achieved through active brazing techniques [74]. In practical application, the enhancement of thermomechanical characteristics within joints often involves a two-step process, where activation and brazing are sequentially conducted. If the geometry of the component allows, applying surface coatings of carbide-forming metals onto CFCs is the favored approach. Subsequently, these components, augmented with metal interlayers, are joined using soft metals during the brazing procedure.

SiC_f/SiC exhibit a reduced susceptibility to oxidative degradation when contrasted with CFCs. In comparison to monolithic SiC, these composites demonstrate heightened resistance against thermal shock, improved impact resistance, and greater fracture toughness. Originally introduced as potential structural components for demonstration power plants [75], SiC_f/SiC have been earmarked for employment in the fusion reactor succeeding ITER. More information on the applications of SiC_f/SiC in fusion structures can be found in [76].

Active brazing found its initial application in the self-joining of SiC_f/SiC against 2000. In this process, a paste-like Si–Ti alloy was employed to bond carburized SiC_f/SiC at a temperature of 1360 °C [77]. Subsequently, Riccardi and colleagues [78,79] extended this technique by brazing SiC_f/SiC together using Si–Ti and Si–Cr filler materials. Their work demonstrated that the formation of Si–Ti, Cr–C, and Si–Cr compounds played a crucial role in enhancing adhesion and achieving strong bonds. Efforts have been made to utilize commercially available Ti-containing Ag-based active brazing alloys for self-joining SiC_f/SiC . One such alloy, Cusin-1 ABA ($(\text{Ag}_{35}\text{Cu})_{97}\text{Ti}_2\text{Sn}_1$), exhibited favorable wetting properties during the self-joining of SiC_f/SiC [80]. A high-temperature shear test was conducted on SiC_f/SiC joints connected using Cusil–ABA ($\text{Ag}_{35.25}\text{Cu}_{1.75}\text{Ti}$). However, it was found that the interface between the reaction-formed TiC layer and the brazing material became the weak point in the joint at elevated temperatures [81]. Notably, the mechanical properties of the joints mentioned above mostly yielded results below 50 MPa when tested at room temperature. This strength falls significantly short of the average strength of the composite materials, indicating that the weakest connect still resides at the joint interface. It is imperative that further endeavors be directed towards enhancing the thermal cycle durability of joints of this nature.

Recent research endeavors have concentrated their efforts on the active brazing of SiC_f/SiC to nickel alloys, as evidenced by studies [82–85]. This approach has yielded commendably high shear strength at room temperature, achieved through the utilization of B-containing active brazing alloys like AuCuTi–B, along with the integration of Mo interlayers, facilitating the bonding of SiC_f/SiC and Hastelloy X [83]. An amalgamation of composite brazing alloys and interlayers has given rise to interfaces that are both functional and intricate in nature. This principle was subsequently reapplied, with researchers adopting a similar strategy. In this instance, Cu foams were employed by Zhang et al. [84]. The aim was to mitigate thermal residual stresses and concurrently enhance the thermomechanical efficiency of the joints. These techniques have found widespread application in various scenarios, such as the joining of materials like alumina and metallic substrates. It should be noted that the copper content within these brazing elements might compromise the oxidation resistance of these joints, particularly at elevated operating temperatures [86,87].

Anheier et al. [88] considered the approach of using interlayers to the active brazing of sapphire viewports in advanced small modular reactors. Optical-based measurement and sensing systems offer significant advantages over traditional instrumentation and control systems employed for monitoring various reactor process parameters, including temperature, flow rate, pressure, and coolant chemistry. External cameras enable the direct and continuous visualization of in-vessel components. While optical access is not integrated into any commercial nuclear power plant or highlighted in reactor designs, successful implementation of optical access has been demonstrated within test reactors.

Prefabricated brazed sapphire viewports are readily available and generally capable of withstanding operating temperatures up to 450 °C and pressures reaching tens of MPa [88]. However, achieving a CTE closely aligned with that of sapphire within the metal viewport flange is essential to ensure the brazed joint can endure complete temperature cycling without failure. Unfortunately, this requirement remains challenging to fulfil. Consequently, connecting viewport windows directly to a metal steel flange through brazing is a rarity. Instead, an intermediary transition metal sleeve, with a closely matched CTE, is brazed onto the sapphire and subsequently laser- or electron-beam welded to the stainless-steel flange [88]. In such cases, brazing alloys based on silver or silver–copper compositions can be employed.

4.2. Nuclear Safety Sensors

In the realm of nuclear reactors, sensors of utmost importance are responsible for real-time measurement of temperature, pressure, coolant level and flow, as well as neutron flux. These sensors are required to exhibit swift responsiveness and heightened sensitivity even when functioning amidst challenging and severe conditions.

4.2.1. Wire-Mesh Multi-Flow Sensors

Wire-mesh sensors are characterized by an extraordinary sensitivity and thus enable the detailed spatial and temporal mapping of flows and especially of multiphase flows [27,28,89]. These sensors, as shown in Figure 6, operate on a foundational concept where measuring points are organized in a grid-like pattern. By placing two distinct sets of wire electrodes perpendicular to one another within a vessel or pipe, the sensor captures the essence of the flow. The procedure involves sequentially activating the transmitting electrodes while concurrently sampling all the receiving electrodes in a parallel fashion. This approach facilitates the assessment of an electrical property (either conductivity or permittivity) of the fluid at each intersection point.

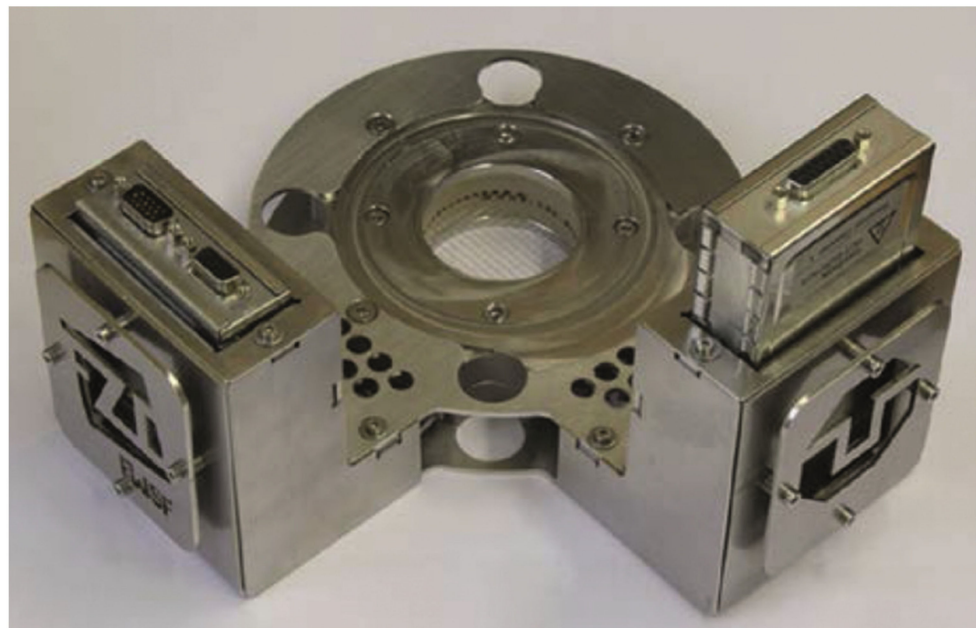


Figure 6. An institute-exclusive hydrothermal grid sensor tailored for the SECA device was developed and allocated within our facilities. The hydrothermal pipe features an inner diameter measuring 60 mm.

The design and production of wire-mesh sensors can be tailored to specific application demands, encompassing a variety of cross-sectional geometries and operational parameters. In parallel, wire-mesh sensors designed for nuclear cooling applications should have the capacity to withstand environmental conditions of up to 400 °C and 10 MPa. Additional requirements for fabrication of wire-mesh sensors are depicted in Figure 7 in a schematic manner. The necessity for accommodating sensors within a confined space contributes to a more compact design. Each electrode's feedthrough exists within the millimeter-scale dimensions. The harsh operational conditions mandate the seamless replacement of faulty feedthroughs. The combination of these stipulations presents significant challenges in the fabrication of the sensors.

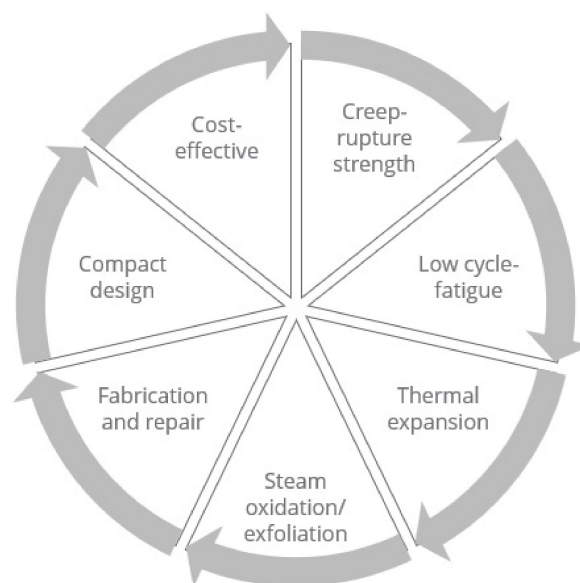


Figure 7. Additional requirements for fabrication of wire-mesh sensors.

Two fundamental approaches have been developed to seal the electrodes effectively. The first involves utilizing polymer sealing materials such as PEEK (polyether ether ketone), PEFT (polytetrafluoroethylene) [29], and the non-electrically conductive epoxy EPO-TEK[®] OE188 [90]. This technique has enjoyed widespread use over an extended period. However, its drawback lies in the limited thermal stability of polymer materials, which confines the sensors to applications below 300 °C.

The alternative method involves brazing alumina by metallizing a section of the surface through the moly-manganese process [91], as shown in Figure 1. This process entails applying a mixture of molybdenum powder and oxides onto the alumina surface. Subsequently, subjecting it to heat treatment exceeding 1200 °C in a wet hydrogen atmosphere triggers the reduction of molybdenum and facilitates interaction between the oxides from both the mixture and the alumina. Upon cooling, this results in the formation of a vitreous phase layer, with the sintered molybdenum powder strongly adhering to the alumina surface. Often, a nickel layer is introduced to enhance the brazing process using conventional filler alloys. This latter design emerges from high-temperature reduction and is particularly suitable for low-temperature applications, notably in cryogenic scenarios. As of now, metallization processes are solely applicable to alumina, and there are no industrial metallization methods in use for non-oxide ceramics.

Employing active brazing techniques holds the potential to significantly broaden the scope of application for wire-mesh sensors. The process of selecting suitable materials for this purpose is outlined in part III. However, it is important to note that Kovar, which is a common material for electrical feedthroughs, is not advised for this application due to its susceptibility to thermohydraulic corrosion.

Owing to pronounced differences in CTE and Young's modulus between high-purity alumina and austenitic stainless steel, such as 316Ti (1.4571), coupled with the elevated yield strength of 316Ti, the prospect of brazing these materials together was initially deemed implausible. It becomes imperative to unearth a novel mechanism that would prevent the complete brazed joint from fracturing during thermal cycles.

Interface patterning creates malleable intrusions in the joints. During thermal cycles, the introduction of malleable intrusions of filler metals serves as a damping mechanism for thermal stress. Drawing from classic fracture mechanics [92], this arrangement substantially bolsters the fracture toughness of the connected interface. As depicted in Figure 8, according to FEM simulation, the intrusions experience the most pronounced plastic deformation [93]. These intrusions act to disrupt the continuous stress lines at the junction interfaces, thereby considerably mitigating significant stress concentrations, unlike the non-patterned specimens.

Further finite element analysis demonstrates that interface patterning effectively modifies the magnitude and even the orientation of torque within the ceramic part of ceramic-metal joints. This adjustment serves to proficiently manage the development of thermal stresses in such joints [93].

In this review, the focus lies on laser active brazing. Despite the myriad benefits associated with this technique, its coverage in the literature has been relatively limited. This is partly attributed to the substantial cost of laser equipment on one hand and, on the other hand, the significant thermal residual stress resulting from the rapid process timeframe. In essence, the brazed components lack sufficient time for the relaxation process to entirely alleviate the residual stress.

To tackle this challenge, TU Dresden has developed two strategies. The initial approach revolves around controlling the peak temperature during the entire brazing process. Given the diverse composition of brazed components—including metals, ceramics, fillers, interfaces, surfaces, and fixtures—it is crucial to leverage the laser's capabilities optimally. The laser device must deliver sufficient energy to melt filler materials while minimizing the temperature of the metallic components within the brazing assembly. This dual objective can effectively reduce the potential for thermal stress induced by the contraction of the metallic components.

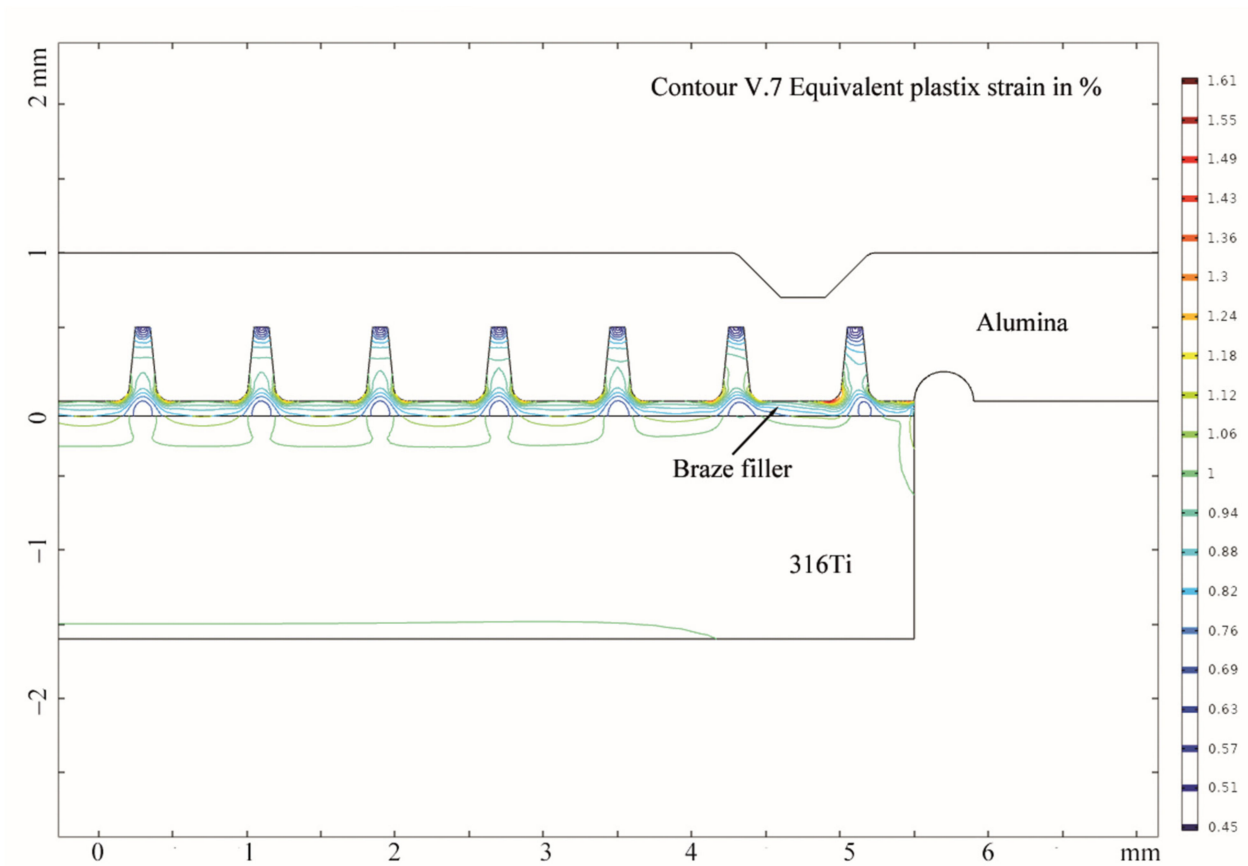


Figure 8. Intrusions undergo the most significant plastic deformation.

The second strategy involves the modification of interfaces, e.g., introducing interface patterning to prevent the fracturing of ceramics. Interface patterning has been realized using nanosecond-pulsed lasers [94]. Careful attention must be paid to avoid microstructural flaws like recast, debris, or extensive remelted areas. This strategic approach alleviates abrupt shifts in elastic properties at the joined interfaces of the brazed components.

4.2.2. Fiber Sensors

Fiber Bragg grating (FBG) stands as a form of distributed Bragg reflector found within a short segment of optical fiber. This specialized structure possesses the ability to reflect specific light wavelengths while allowing all others to pass through. The utilization of heat-resistant FBG sensors for seismic monitoring is of utmost importance for nuclear plants. When considering the integration of FBG sensors into engineering plants or nuclear facilities, a pivotal factor to account for is the operational temperature.

The temperature of the outlet coolant plays a decisive role in determining the overall efficiency of power plants. The outlet temperature of the coolant plays a decisive role in determining the overall efficiency of power plants. The highest temperature requirements are placed on gas-cooled high-temperature requirements, in which the outlet temperature of the helium can be up to 900 °C [95]. In sodium-cooled reactors, the temperature of the liquid sodium in the primary cooling circuit can rise to up to 550 °C [96]. Such extreme temperatures can lead to creep fatigue in materials such as AISI 316 (1.4401). In light water reactors, the coolant temperatures are in the range between 250 and 350 °C [97].

From a practical perspective, concerning the installation of FBG sensors within nuclear facilities, the optimal choice could be active brazing, particularly utilizing techniques like RAB. Within nuclear facilities, personnel are required to engage in intricate tasks involving the attachment of FBG sensors, all while donning radiation-protection suits and gloves, adding a layer of complexity to the process. The presence of a convenient laser torch or

induction heater becomes indispensable for precise, localized heating. Ongoing research endeavors are addressing this matter, but only a limited number of references delve into this subject. For instance, Sandin et al. [98] employed Cusin-1 ABA to hermetically seal an Ni-coated fiber within a transducer body crafted from Inconel 600. The brazed transducer successfully withstood rigorous high-temperature thermal cycling tests for nearly six months, exhibiting no failures upon completion of the testing phase.

4.3. Hydrogen Devices

Given the multitude of hydrogen sensors available in the market, consumers have a wide array of choices to suit their specific needs. Nonetheless, determining the most suitable sensor technology can be intricate. Within the scope of this review, we exclusively focus on electrochemical and thermal conductivity sensors utilizing polymer or silicon substrates, primarily fabricated through screen printing.

4.3.1. Ceramic-Based Pressure Sensors

Traditional pressure sensors that rely on silicon and silicon-on-insulator technology are limited to functioning effectively at temperatures ranging between 200 °C and 300 °C. For applications requiring higher temperatures, such as those in elevated temperature environments, the production of high-temperature pressure sensors primarily employs two technologies: low-temperature co-fired ceramic (LTCC) and high-temperature co-fired ceramic (HTCC). These methods involve complex procedures like multilayer ceramic and lamination processes, high-temperature sintering, and screen-printing techniques.

However, these approaches face challenges due to differences in CTEs between LTCC/HTCC materials and steel housings. As a result, they are intricate and susceptible to vulnerabilities, potentially leading to deformations or collapse of the sealed cavity within the sensor. To address these issues, a solution was developed involving a gradual integration of LTCC/HTCC-based sensor components into steel connectors [99].

The encapsulation concept is illustrated in Figure 9, and the encapsulation process can be divided into three distinct steps. In step A, a Kovar substrate with a CTE closely matched to Al₂O₃ is connected to the steel connector using methods like electron beam welding or direct brazing. The subsequent step B involves joining Kovar and Al₂O₃ through active brazing, a technique that has undergone extensive research. The final step, step C, focuses on creating ceramic–ceramic joints using a glass-based sealant or other applicable techniques.



Figure 9. Diagram depicting the progressive integration process of an LTCC sensor into the steel connector.

An alternative approach involves connecting Kovar and LTCC during step B. While LTCC exhibits better electrical properties compared to alumina, the brazing of LTCC has received limited attention in the literature, lacking comprehensive systematic findings. To address this challenge, intricate multi-layer thin-film metallization techniques are often employed. In one method, Kovar caps with gold plating were directly brazed onto a multi-layer thin-film structure composed of Ti/Mo/Cu/Ni/Au, where the Ti film was sputtered onto the LTCC [100].

Another approach, as demonstrated by Alcatel Alenia Space Italia, employs Au–Sn alloys for brazing Kovar and LTCC together. In this method, both materials are coated with a layer of gold film [101]. Walker et al. [102] successfully united Kovar and LTCC

using active brazing alloys such as Incusil–ABA coupled with Ti–Pt thin-film metallization. These brazing techniques exhibited exceptional hermeticity, and the metallized samples displayed heightened tensile strength. Notably, the surface quality of the LTCC significantly influenced performance in tensile and helium leak testing. The most favorable outcomes were observed when surfaces were ground and subsequently refired to repair microcracks. Schilm et al. [99] explored the usage of three distinct commercial active brazing alloys for connecting Kovar to LTCC. Early results are promising, with some level of hermeticity achieved; the focus now shifts to controlling intermetallic formation in subsequent stages.

4.3.2. SOEC/SOFC

In recent years, there has been a notable surge in research focused on the production of hydrogen through advanced high-temperature electrolysis techniques. Among these methods, one prominent approach is the utilization of solid oxide electrolyzer cells (SOECs) [103] in a process akin to reversing the polarity of solid oxide fuel cells (SOFCs). Stacked small cells are joined together to produce hydrogen for external work. These devices lend themselves to convenient modularization and seamless digital integration and are poised to assume a pivotal role in the prospective hydrogen-based economy. While the sealing of components remains a persistent challenge for developers working on SOFC stacks, it becomes an even more formidable issue when dealing with solid oxide stacks designed for high-temperature steam electrolysis aimed at hydrogen generation. One of the main problems of hydrogen electrolysis is the small size of the hydrogen molecules, which can swiftly escape via high-temperature collection channels.

This review centers on the examination of sealing technologies pertinent to planar SOFCs, encompassing those that have been under consideration, are presently in use, or are currently being explored. In numerous cases, the seal is positioned between the yttria-stabilized zirconia (YSZ) electrolyte and a high-temperature metal frame, with its exposure to operational temperatures ranging approximately from 750 to 850 °C. Within SOFCs, this seal consistently encounters an oxidizing atmosphere on the cathode side (such as air), and on the anode side, it faces a fuel gas comprising diverse proportions of hydrocarbons (e.g., CH₄), H₂, CO, CO₂, and H₂O. In the context of SOECs, the polarity is reversed: The cathode transitions to the anode, and conversely, the anode becomes the cathode. The typical electrode materials will likely remain unchanged unless extended endurance tests necessitate a modification in materials.

During operation, it is imperative that the seals remain hermetically intact for extended durations, spanning thousands of hours. Various sealing techniques are under consideration, including active brazing, glass seals, composite seals, and mechanical seals. Each of these methods possesses distinct strengths and weaknesses [104]. Active metal brazing typically requires a low-oxygen partial pressure, which poses challenges for perovskite materials. Glass seals exhibit comparatively lower strength and exhibit a gradual but consistent degradation over time. Elastic composite seals lack long-term stability.

Within the brazing community, significant attention is directed towards the development of techniques for joining SOEC/SOFCs, with a particular focus on the reactive air-brazing (RAB) process [104,105]. RAB represents a variation of active brazing conducted in an air environment, utilizing an oxidation-resistant composite braze filler metal. It developed from “direct copper bonding” [106], which has been known since the 1960s. Currently, research predominantly centers around the application of silver-based braze filler metals containing varying proportions of copper oxide and occasionally incorporating minor quantities of titanium oxide or other elements/compounds. These investigations aim to facilitate the joining of SOEC/SOFCs materials like YSZ ceramics or ferritic steels, as shown in Table 3. Indeed, any oxides that are thermodynamically stable and exhibit minimal coarsening tendencies can be utilized in these composite fillers. The principles governing metal matrix composites can be employed to tailor the CTEs of the final filler materials, like the Ag–Al₂TiO₅ system. It has been recognized that the interaction between filler metals and substrates through chemical diffusion could potentially compromise the performance

of the base materials. As a result, efforts have been made to limit interdiffusion by using diffusion barriers. For instance, Zhou et al. [60] applied an aluminum coating to Crofer22H, while Si et al. [62] utilized Mn–Co spinel-coated Crofer22APU as their substrates.

In further investigations, an effective adhesion has been achieved between interconnected components, even under exceedingly high operational temperatures. This has minimized the deterioration of the brazed elements to a certain extent; at the same time, the gas tightness has been increased even under substantial pressure differentials. Enhancements have been implemented to address the unacceptable decline in strength and gas tightness during prolonged periods of stationary service as well as during start–stop cycles [8,60,107]. The RAB process has a significant drawback wherein it introduces an excessive amount of oxygen into the brazed joint. This frequently results in elevated porosity, which in turn compromises the joint’s gas tightness, corrosion resistance, and overall strength. The use of brazing pastes appears to significantly contribute to the formation of these pores. Moreover, porosity may arise due to interactions between the filler metal, particularly metal oxides, and the base material. However, a comprehensive analysis of this phenomenon is currently lacking.

4.4. Thermoelectric Generators (TEGs)

A thermoelectric module designed for high-temperature applications primarily operates within a vacuum or under protective gas conditions. Some TEGs operate in an ambient atmosphere and are used to supply power to measuring devices that provide information on the actual temperature of power plants in the case of a power failure. The schematic representation of such a device is presented in Figure 10. This device incorporates multiple n-type TiO_x legs and p-type B_xC legs affixed to stable insulating substrates (AlN). These substrates feature a structured metallization layer (crafted from Kovar) that enables flexible electrical interconnection of individual legs, whether in series or parallel configuration. These substrates are subsequently linked to heat exchangers.

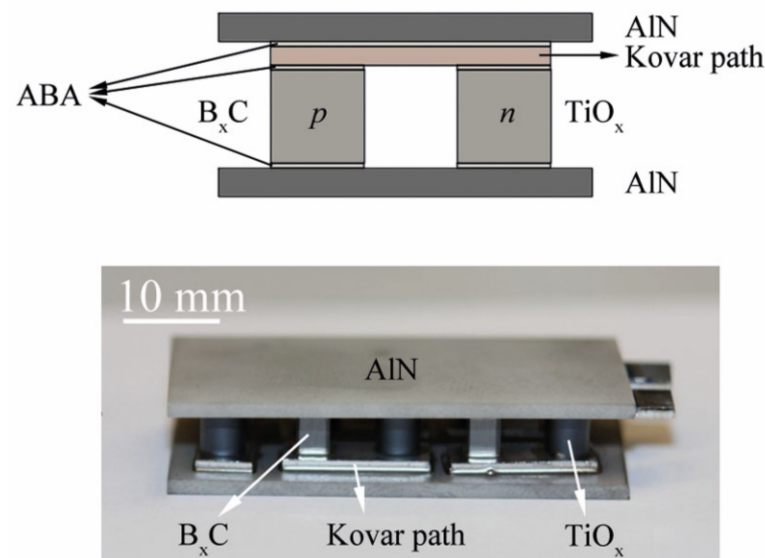


Figure 10. Diagram illustrating a TiO_x – B_xC thermoelectric module. Image supported by A.-M. Reinecke.

Diverging from conventional non-oxide thermoelectric materials, TiO_x is a ceramic substance that conventional brazing alloys cannot effectively adhere during brazing procedures. However, through the utilization of active metal brazes, it is possible to directly bond such ceramic materials with metals. In thermoelectric applications, these bonds must not only exhibit satisfactory mechanical stability but also demonstrate low electrical resistance and excellent thermal conductivity to minimize energy losses [108–110]. Due

to the instability of TiO_x ceramic stoichiometry at elevated temperatures in air, the use of active metal brazing under protective atmosphere is well suited for this purpose. It should be noted that Ag-containing ABAs are generally not used for TEGs, as silver diffuses into the semiconductor ceramic and thus degrades its properties.

Feng et al. [111] employed laser active brazing in their brazing approach. The localized heat input and brief process duration render the laser-assisted technique highly appealing for ceramic–metal brazing. However, only a limited number of sources discuss laser active brazing. An issue arises from elevated contact resistance, as evidenced by the assessment of the thermoelectric module’s overall electrical resistance. The question of how to effectively mitigate non-ohmic contacts at the brazement still remains an unresolved challenge. However, Conze et al. [108] utilized active metal brazing to metallize AlN substrates. The adoption of the active metal-brazing method provides the flexibility to easily switch between copper and alternative metals like nickel, tungsten, or molybdenum. This versatility stands as a significant advantage of the process.

5. Brazement Degradation

Test data from laboratory experiments lasting several hundred hours are often published. This test duration is short compared to the intended lifetime of energy reactors (e.g., a lifetime of >40,000 h for a SOEC/SOFC stack [112]) and does not represent the real scale of degradation processes. This publication is intended to stimulate a broader exchange with initial findings. At the center of this discourse are three key dimensions: design considerations, transport implications, and the mechanical aspects of the issue.

5.1. Design Aspects

To establish a robust brazing process, meticulous material selection must be followed by a comprehensive design of the brazed joint, employing finite element method (FEM) assistance. Ensuring a dependable brazed joint involves the consideration of the subsequent design facets.

The first aspect pertains to geometry. Analogous to fatigue design principles, it is imperative to steer clear of sharp edges and corners. For instance, forming circular connections through brazing proves more manageable than achieving the same with rectangular ones. Given that the post-brazing thermal stress within ceramics predominantly stems from the contraction of metal components, the relative thickness of metal and ceramics assumes a pivotal role in determining stress concentration in vulnerable zones. The thickness of the brazed material impacts the alleviation of thermal stress, albeit under specific conditions. Moreover, the pre-brazing residual stress state of the metals directly influences the outcomes of the brazing process.

The second facet concerns thermal stress considerations. It is important to recognize that mismatches in CTE are not the sole contributors to thermal stresses. Substantial volume alterations arising from phase transitions, marked shifts in elastic properties at interfaces, and significant fluctuations in defect density—particularly in ceramic materials during a laser process—can all contribute significantly to these stresses. In the context of design, striving for controlled and uniform heat distribution along with a gradual transition in material properties throughout the brazed joint remains a consistent objective.

Furthermore, the role of ceramics in the brazing process is of paramount importance. Given the inherently low fracture toughness of ceramics, the presence of microcracks on their surface can engender significant fissures within the ceramic structure, thereby compromising the reliability of the joints formed. Consequently, flaws within the ceramic must be avoided or limited to a size of a few micrometers, which is comparable to the size of pores [10]. It is advantageous to use ceramic material with a high surface quality for brazing purposes.

Moreover, the complexity of the ceramic manufacturing process leads to comparatively large property fluctuations that affect the performance of the brazed joints.

5.2. Transport Aspects

The primary degradation mechanisms observed in active brazed joints for energy applications are closely tied to the transport properties of diffusive elements. As many ABAs are silver-based, the exceptional conductivity of silver when it comes to oxygen and hydrogen poses a challenge to the long-term stability of these joints.

The initial consequence of this challenge is that exposing silver to both reducing and oxidizing environments concurrently, particularly at elevated temperatures even at 500 °C, triggers extensive pore development within the bulk silver. This pore formation predominantly occurs along the grain boundaries, where diffusion transpires at a faster rate compared to within the bulk material. This phenomenon is attributed to the nucleation and growth of high-pressure steam bubbles that eventually coalesce to create pores and fissures within the silver, leading to the formation of water vapor.

The subsequent impact of silver's robust oxygen and hydrogen conductivity lies in its capacity to accelerate the process of inter-diffusion at joint interfaces. This acceleration, in turn, expedites the creation of intermetallic compounds, gas-filled pores, and even Kirkendall voids. It is worth noting that, in accordance with Arrhenius' law, the concentration of vacancies within all metallic materials increases with rising temperatures. As a result, the expedited inter-diffusion at elevated temperatures emerges as a prevalent issue across various metallic fillers.

Should Cu be a participant in the ABA process, the oxidation of Cu could serve as a predominant factor in high-temperature oxidation. Just as observed in traditional ABA scenarios subsequent to the initial stage, Cu tends to distribute primarily as a eutectic phase alongside Ag in joints or forms mixed oxides in conjunction with reactive elements at interfaces. Subsequent to the oxidation process, the presence of coarse CuO phases contributes to the weakening and deterioration of the joint integrity.

Conversely, in the context of reactive air brazing (RAB), CuO finds utility within composite fillers. Following the findings of Weil et al. [7], the microstructure of the brazed joint appears to remain relatively consistent when exposed to 750 °C air for up to 800 h in a system involving 5YSZ/Ag-CuO/Crofer22APU (W.-Nr. 1.4760). The introduction of moist hydrogen prompts internal CuO precipitates within the filler material to undergo reduction into metallic copper, accompanied by the formation of vapor bubbles due to water precipitation. This complete reduction process takes place within a 200 h exposure at 750 °C. Schilm et al. [18] demonstrated the development of intricate oxidic interfacial layers and Kirkendall voids when a 3YSZ/Ag-CuO/Crofer22APU system was subjected to 850 °C air for up to 800 h of isothermal exposure.

The presence of oxygen and hydrogen within silver significantly influences the way in which the microstructure of Ti and its oxides evolve. Ti contributes to an elevated melting point and enhanced fluidity, consequently augmenting the wetting capabilities of ABA. However, there exist conflicting viewpoints in the literature regarding the utilization of Ti-containing ABAs in SOEC/SOFC applications. When Ti-containing ABAs are employed in brazing, they tend to yield brittle reaction products at interfaces due to Ti triggering excessive and drastic interfacial reactions, as indicated by Woirgard et al. [113]. Kiebach et al. [114], on the other hand, advocated for the use of Ti-free brazing alloys in SOEC/SOFC applications, as the Ti phases formed after sealing with silver-ABA are not stable under the operating conditions encountered within cells. This instability manifests through three primary issues: the dynamic evolution of TiO_x , agglomeration of Ti-Fe, and the establishment of mixed oxide equilibria.

In future endeavors, to curtail the conduction of oxygen and hydrogen, Ag-based active brazing alloys containing grain-boundary stabilizers like Al or Nb can be considered. To mitigate inter-diffusion, the application of diffusion barrier coatings on the metallic part's surface prior to brazing can be explored. It is advisable to keep the Ti content at a sufficiently low level to enhance resistance to aging. It is important to note that the concurrent use of Cu and Ti is not recommended in oxidizing or dual-atmosphere conditions.

5.3. Thermal Cycles Aspects

Under cyclic thermal loads, the structural response of active-brazed connections becomes a multifaceted phenomenon that is increasingly pivotal in the design of energy sensors and reactors, among other applications.

One of the most prevalent failure modes stemming from the repeated thermal cycling of sandwiched joints is the formation of microcracks at the bonding interfaces. This issue primarily stems from the non-uniformity arising due to the differences in CTEs among the various materials involved, including metals, ceramics, and ABAs. Localized stress concentrations within the ceramic components and the exposed edge interfaces serve as potential focal points for the initiation of these microcracks. Depending on the specific geometric configuration and loading conditions, these critical regions may incite damage and interact with various modes of failure, giving rise to intricate failure patterns within active-brazed structures.

It is imperative to embed intrinsic mechanisms within active-brazed connections to enhance their resistance to thermal cycling. Neglecting the incorporation of such mechanisms can result in premature joint failure. For example, Weil et al. [7] employed Ag–4CuO fillers in their experiments involving thermal cycling spanning from ambient temperature to 750 °C. Notably, the specimens produced through reactive active brazing exhibited initial indications of delamination along the braze-to-electrolyte interface after 50 cycles. Additionally, TEGs (thermoelectric generators) manufactured using active brazing were subjected to thermal cycles ranging from 60 °C to 440 °C by Martin et al. [109]. In this case, severe cracking became evident in the cross-sectional analysis of the TiO_x module's hot side after 1000 cycles. It is worth highlighting that all these cracks initiated at stress concentration points and propagated deeper into the ceramics or adjacent interfaces.

Numerous approaches have been undertaken to ameliorate this situation, with the foremost technique involving the utilization of soft interlayers. Employing soft interlayers, characterized by low yield strength, serves a dual purpose. Firstly, they alleviate stress through plastic deformation, and secondly, they act as a barrier to hinder element diffusion and the formation of brittle intermetallic compounds. This dual action leads to enhancements in the mechanical properties and thermal cycling durability of the connections. For instance, Zhu et al. [51] utilized Ag–Cu–Ti/Cu/Ag–Cu composite fillers during thermal cycling spanning from 0 °C to 500 °C, demonstrating the effectiveness of this approach. Additionally, Qiao et al. [115] demonstrated that Ni/Ti/Ni interlayers could alleviate residual stresses in alumina/Kovar joints during initial thermal cycles and positively influence the shear stress within the joints.

Another avenue to bolster thermal cycle resistance is the incorporation of a porous matrix. In one instance, porous graphite was actively brazed to alumina [116]. Remarkably, the presence of whisker phases within the graphite pores prevented the occurrence of cracks or any other defects at the joint interfaces even after subjecting them to 100 thermal cycles ranging from 30 to 600 °C. A pre-patterned matrix is expected to work in the same way.

While comprehensive material characterization, mechanical testing, and design validation studies—such as thermal cycling and vacuum testing—are essential for specific mission assurance, it is unfeasible to experimentally predict the structural integrity of a wide array of energy structures exposed to diverse thermomechanical loading scenarios. Hence, it proves advantageous to develop enhanced models and analytical tools to gain a deeper understanding of the thermal stability and damage tolerance of intricate brazed structures, enabling an improved prediction of their remaining useful lifespan.

6. Closing Remarks

Active brazing enables the direct bonding of metal to ceramic, eliminating the need for metallization. This streamlines the joining process, resulting in a robust hermetic seal capable of withstanding elevated operational temperatures. It opens up new possibilities for joining previously incompatible materials and components, making it particularly advantageous in applications involving sensors and reactors. In the present review, the

fundamental principles of active brazing are reiterated, and a typical method for materials selection is outlined. Viable solutions for energy sensor encapsulation and reactor sealing are summarized. An analysis is conducted on the key factors significantly impacting brazement degradation.

The following outlines several emerging areas in active brazing concerning energy devices sealing. Active brazing is gaining significant traction in industrial applications due to its automation-friendly nature and the ability to join dissimilar materials. The integration of active brazing with advanced industrial manufacturing techniques such as hybrid active weld brazing and fiber laser active brazing is becoming increasingly crucial.

Hybrid active weld brazing minimizes heat input on the substrate through controlled power supply. This results in a small heat-affected zone and minimal mixing of brazing materials and substrates. On the other hand, fiber laser active brazing offers precise control, low heat input, and reduced power consumption. It is the ideal choice for working with very small components and intricate structures. However, a fundamental understanding and mastery of laser active brazing are imperative for further advancing these two methods. There is still a need for systematic research in these emerging areas. In addition to advancing the integration of active brazing with advanced laser processing techniques, there is a need for breakthroughs in direct metallization for thick films using active brazing. Moreover, achieving mass production of micron electronic components and sensors by using laser active brazing is crucial for further progress.

In the context of energy devices sealing, two critical considerations are paramount for the safe application of active brazing. First, the design must account for thermal cycling challenges. In addition to employing basic principles such as soft interlayers and functional composite ABAs, researchers should delve into investigating interface and surface patterning techniques.

Secondly, research efforts should be directed towards developing active joints suitable for extreme environments. This entails the creation of highly ductile ABAs with controlled expansion at elevated service temperatures and exceptional resistance to water vapor. Overall, these endeavors represent significant strides in the field of active brazing, with the potential to revolutionize energy devices sealing.

Author Contributions: Conceptualization, J.F.; writing—original draft preparation, J.F.; writing—review and editing, M.H. and A.-M.R.; supervision, A.H.; project administration, M.H. All authors have read and agreed to the published version of the manuscript.

Funding: The project on which this publication is based was funded by the Germany BMBF under grant number 02NUK068A. The responsibility for the content of this publication lies with the authors.

Data Availability Statement: The data presented in this study are available on request from the corresponding author. The data are not publicly available due to restrictions.

Conflicts of Interest: The authors declare no conflicts of interest.

References

1. Weber, F. *Konflikte um Die Energiewende*; Springer: Wiesbaden, Germany, 2018. (In German)
2. Elssner, G.; Petzow, G. Metal/Ceramic Joining. *ISIJ Int.* **1990**, *30*, 1011–1032. [[CrossRef](#)]
3. Elssner, G.; Petzow, G. Verträglichkeit zwischen Materialkomponenten in Metall-Keramik-Verbundwerkstoffen. *Int. J. Mater. Res.* **1973**, *64*, 280–286. (In German) [[CrossRef](#)]
4. Wang, G.; Lannutti, J.J. Chemical thermodynamics as a predictive tool in the reactive metal brazing of ceramics. *Metall. Mater. Trans. A* **1995**, *26*, 1499–1505. [[CrossRef](#)]
5. Mishra, S.; Sharma, A.; Jung, D.H.; Jung, J.P. Recent Advances in Active Metal Brazing of Ceramics and Process. *Met. Mater. Int.* **2020**, *26*, 1087–1098. [[CrossRef](#)]
6. Peteves, S.D.; Paulasto, M.; Ceccone, G.; Stamos, V. The reactive route to ceramic joining: Fabrication, interfacial chemistry and joint properties. *Acta Mater.* **1998**, *46*, 2407–2414. [[CrossRef](#)]
7. Weil, K.S.; Coyle, C.A.; Darsell, J.T.; Xia, G.G.; Hardy, J.S. Effects of thermal cycling and thermal aging on the hermeticity and strength of silver–copper oxide air-brazed seals. *J. Power Sources* **2005**, *152*, 97–104. [[CrossRef](#)]
8. Waetzig, K.; Schilm, J.; Mosch, S.; Tillmann, W.; Eilers, A.; Wojarski, L. Influence of the Brazing Paste Composition on the Wetting Behavior of Reactive Air Brazed Metal–Ceramic Joints. *Adv. Eng. Mater.* **2021**, *23*, 2000711. [[CrossRef](#)]

9. Li, C.C.; Kuhn, B.; Brandenburg, J.; Beck, T.; Singheiser, L.; Bobzin, K.; Bagcivan, N.; Kopp, N. Improving Contour Accuracy and Strength of Reactive Air Brazed (RAB) Ceramic/Metal Joints by Controlling Interface Microstructure. *Adv. Eng. Mater.* **2012**, *14*, 394–399. [[CrossRef](#)]
10. Akselsen, O.M. Advances in brazing of ceramics. *J. Mater. Sci.* **1992**, *27*, 1989–2000. [[CrossRef](#)]
11. Walker, C.A.; Hodges, V.C. Comparing metal-ceramic brazing methods. *Weld. J.* **2008**, *87*, 43–50.
12. Passerone, A.; Muolo, M.L. Joining Technology in Metal-Ceramic Systems. *Mater. Manuf. Process.* **2000**, *15*, 631–648. [[CrossRef](#)]
13. Fernie, J.A.; Drew, R.A.L.; Knowles, K.M. Joining of engineering ceramics. *Int. Mater. Rev.* **2009**, *54*, 283–331. [[CrossRef](#)]
14. Sivaprahasam, D.; Sujitha, T.; Gowtham, U.; Jayachandran, B.; Gopalan, R. Microstructure and heat transfer characteristics of active brazed Ceramic–Metal joints. *Ceram. Int.* **2021**, *47*, 16133–16140. [[CrossRef](#)]
15. Kassam, T.A. *A Review of the Alumina/Ag-Cu-Ti Active Metal Brazing Process*; CRC Press: Boca Raton, FL, USA, 2018; p. 256.
16. Asthana, R.; Singh, M. 11—Active metal brazing of advanced ceramic composites to metallic systems. In *Advances in Brazing*; Sekulić, D.P., Ed.; Woodhead Publishing: Sawston, UK, 2013; pp. 323–360.
17. Weil, K.S. The state-of-the-art in sealing technology for solid oxide fuel cells. *JOM* **2006**, *58*, 37–44. [[CrossRef](#)]
18. Schilm, J.; Rost, A.; Poenicke, A.; Kusnezoff, M.; Michaelis, A. Ceramic Integration Technologies for Solid Oxide Fuel Cells. *Int. J. Appl. Ceram. Technol.* **2012**, *9*, 688–699. [[CrossRef](#)]
19. Fernie, J.A.; Hanson, W.B. Best practice for producing ceramic-metal bonds. *Ind. Ceram.* **1999**, *19*, 172–175. (In Italian)
20. Walker, C.A.; Bishop, G.; De Smet, D.J. *Single and Double Reaction Layer Formation Using Reduced Active Element Containing Brazing Filler Metals*; Sandia National Lab (SNL-NM): Albuquerque, NM, USA, 2015.
21. Walker, C.A. 16—Metal–nonmetal brazing for electrical, packaging and structural applications. In *Advances in Brazing*; Sekulić, D.P., Ed.; Woodhead Publishing: Sawston, UK, 2013; pp. 498–524.
22. Lugscheider, E.; Tillmann, W. Development of new active filler metals in a Ag–Cu–Hf system. *Weld. J. Res. Suppl.* **1990**, *69*, 416–421.
23. Bellosi, A.; Kosmac, T.; Tomsia, A.P. *Interfacial Science in Ceramic Joining*; Springer Science & Business Media: Dordrecht, The Netherlands, 1998; Volume 58.
24. Bobzin, K.; Kopp, N.; Wiesner, S. Influence of Filler and Base Material on the Pore Development during Reactive Air Brazing. *Adv. Eng. Mater.* **2014**, *16*, 1456–1461. [[CrossRef](#)]
25. Pönicke, A.; Schilm, J.; Kusnezoff, M.; Michaelis, A. Aging Behavior of Reactive Air Brazed Seals for SOFC. *Fuel Cells* **2015**, *15*, 735–741. [[CrossRef](#)]
26. Kim, J.Y.; Hardy, J.S.; Weil, K.S. Effects of CuO Content on the Wetting Behavior and Mechanical Properties of a Ag–CuO Braze for Ceramic Joining. *J. Am. Ceram. Soc.* **2005**, *88*, 2521–2527. [[CrossRef](#)]
27. Pietruske, H.; Prasser, H.M. Wire-mesh sensors for high-resolving two-phase flow studies at high pressures and temperatures. *Flow Meas. Instrum.* **2007**, *18*, 87–94. [[CrossRef](#)]
28. Hampel, U.; Otahal, J.; Boden, S.; Beyer, M.; Schleicher, E.; Zimmermann, W.; Jicha, M. Miniature conductivity wire-mesh sensor for gas-liquid two-phase flow measurement. *Flow Meas. Instrum.* **2009**, *20*, 15–21. [[CrossRef](#)]
29. Lucas, D.; Beyer, M.; Krepper, E. *TOPFLOW-Experiments, Development and Validation of CFD Models for Steam-Water Flows with Phase Transfer. Final Report; TOPFLOW-Experimente, Modellentwicklung und Validierung von CFD-Codes fuer Wasser-Dampf-Stroemungen mit Phasenuebergang. Abschlussbericht*; Helmholtz-Zentrum Dresden-Rossendorf Institut für Sicherheitsforschung; Dresden, Germany, 2011. (In German)
30. Hosemann, P.; Frazer, D.; Fratoni, M.; Bolind, A.; Ashby, M.F. Materials selection for nuclear applications: Challenges and opportunities. *Scr. Mater.* **2018**, *143*, 181–187. [[CrossRef](#)]
31. Hwang, C.L.; Yoon, K.S. *Multiple Attribute Decision Making Methods and Applications: A State-of-the-Art Survey*; Springer: Berlin/Heidelberg, Germany, 1981; p. 269.
32. Klemm, H.; Fritsch, M.; Schenk, B. Corrosion of Ceramic Materials in Hot Gas Environment. In *28th International Conference on Advanced Ceramics and Composites B: Ceramic Engineering and Science Proceedings*; Lara-Curzio, E., Readey, M.J., Eds.; The American Ceramics Society: Columbus, OH, USA, 2004; Volume 25, pp. 463–468.
33. Opila, E.J.; Jacobson, N.S.; Myers, D.L.; Copland, E.H. Predicting oxide stability in high-temperature water vapor. *JOM* **2006**, *58*, 22–28. [[CrossRef](#)]
34. Ueno, S.; Jayaseelan, D.D.; Ohji, T. Development of Oxide-Based EBC for Silicon Nitride. *Int. J. Appl. Ceram. Technol.* **2004**, *1*, 362–373. [[CrossRef](#)]
35. Louthan, M.R.; Caskey, G.R.; Donovan, J.A.; Rawl, D.E. Hydrogen embrittlement of metals. *Mater. Sci. Eng.* **1972**, *10*, 357–368. [[CrossRef](#)]
36. Tucker, M.C.; Jacobson, C.P.; De Jonghe, L.C.; Visco, S.J. A braze system for sealing metal-supported solid oxide fuel cells. *J. Power Sources* **2006**, *160*, 1049–1057. [[CrossRef](#)]
37. Kobsiriphat, W.; Barnett, S. Ag–Cu–Ti Braze Materials for Sealing SOFCs. *J. Fuel Cell Sci. Technol.* **2008**, *5*, 011002. [[CrossRef](#)]
38. Schaefer, R.P.; Flynn, J.E.; Doyle, J.R. Brazing filler metal evaluation for an aircraft gas turbine engine application. *Weld. J.* **1971**, *50*, 394s–400s.
39. Xian, A.P.; Si, Z.Y.; Zhou, L.J.; Shen, J.N.; Li, T.F. An improvement of the oxidation resistance of Ag–Cu eutectic-5 at% Ti brazing alloy for metal/ceramic joints. *Mater. Lett.* **1991**, *12*, 84–88. [[CrossRef](#)]
40. Beeranur, R.; Waghmare, K.K.; Singh, R.k. Characterization of Vacuum Brazing of SS 304 and Alumina Ceramic with Active Brazing Alloy. *Procedia Mater. Sci.* **2014**, *5*, 969–977. [[CrossRef](#)]

41. Zhu, M.G.; Chung, D.D.L. Improving the strength of brazed joints to alumina by adding carbon fibres. *J. Mater. Sci.* **1997**, *32*, 5321–5333. [[CrossRef](#)]
42. Lee, K.-Y. Brazing ceramic to stainless steel enhanced by surface modification. *Weld. J.* **2007**, *86*, 35.
43. Su, C.Y.; Zhuang, X.Z.; Pan, C.T. Al₂O₃/SUS304 Brazing via AgCuTi-W Composite as Active Filler. *J. Mater. Eng. Perform.* **2014**, *23*, 906–911. [[CrossRef](#)]
44. Haferkamp, H.; Bach, F.; von Alvensleben, F.; Kreutzburg, K. *Laser Beam Active Brazing of Metal Ceramic Joints*; SPIE: Bellingham, WA, USA, 1996; Volume 2703.
45. Sun, R.J.; Zhu, Y.; Guo, W.; Peng, P.; Li, L.H.; Zhang, Y.; Fu, J.; Li, F.; Zhang, L.X. Microstructural evolution and thermal stress relaxation of Al₂O₃/1Cr18Ni9Ti brazed joints with nickel foam. *Vacuum* **2018**, *148*, 18–26. [[CrossRef](#)]
46. Yang, Z.W.; Yang, J.H.; Han, Y.J.; Wang, Y.; Wang, D.P. Microstructure and mechanical properties of 17-4PH stainless steel and Al₂O₃ ceramic joints brazed with graphene reinforced Ag-Cu-Ti brazing alloy. *Vacuum* **2020**, *181*, 109604. [[CrossRef](#)]
47. Südmeyer, I.; Rohde, M.; Besser, H.; Grein, M.; Liesching, B.; Schneider, J. *The Effect of a Homogenizing Optic on Residual Stresses and Shear Strength of Laser Brazed Ceramic/Steel-Joints*; SPIE: Bellingham, WA, USA, 2011; Volume 7921.
48. Rohde, M.; Südmeyer, I.; Urbanek, A.; Torge, M. Joining of alumina and steel by a laser supported brazing process. *Ceram. Int.* **2009**, *35*, 333–337. [[CrossRef](#)]
49. Cao, Y.; Yan, J.; Li, N.; Zheng, Y.; Xin, C. Effects of brazing temperature on microstructure and mechanical performance of Al₂O₃/AgCuTi/Fe-Ni-Co brazed joints. *J. Alloys Compd.* **2015**, *650*, 30–36. [[CrossRef](#)]
50. Ali, M.; Knowles, K.M.; Mallinson, P.M.; Fernie, J.A. Evolution of the interfacial phases in Al₂O₃-Kovar[®] joints brazed using a Ag-Cu-Ti-based alloy. *Philos. Mag.* **2017**, *97*, 718–742. [[CrossRef](#)]
51. Zhu, Q.Y.; Li, S.H.; Hu, K.J.; Liang, X.W.; Cai, Y.Y.; Liu, Z.; Zhang, Y. Enhanced mechanical properties and thermal cycling stability of Al₂O₃-4J42 joints brazed using Ag-Cu-Ti/Cu/Ag-Cu composite filler. *Ceram. Int.* **2021**, *47*, 30247–30255. [[CrossRef](#)]
52. Fukaya, Y.; Kobayashi, T.; Hirai. Joining of Al₂O₃ and steel using a Cu₂O + Cu + Ag-Cu-Ti joining method. *Weld. Int.* **1991**, *5*, 230–235. [[CrossRef](#)]
53. Niu, G.B.; Wang, D.P.; Yang, Z.W.; Wang, Y. Microstructure and mechanical properties of Al₂O₃ ceramic and TiAl alloy joints brazed with Ag-Cu-Ti filler metal. *Ceram. Int.* **2016**, *42*, 6924–6934. [[CrossRef](#)]
54. Lin, K.L.; Singh, M.; Asthana, R.; Lin, C.H. Interfacial and mechanical characterization of yttria-stabilized zirconia (YSZ) to stainless steel joints fabricated using Ag-Cu-Ti interlayers. *Ceram. Int.* **2014**, *40*, 2063–2071. [[CrossRef](#)]
55. Huang, L.W.; Wu, Y.Y.; Shiue, R.K. The effect of oxygen pressure in active brazing 8YSZ and Crofer 22H alloy. *J. Mater. Res. Technol.* **2021**, *10*, 1382–1388. [[CrossRef](#)]
56. Bobzin, K.; Schlaefel, T.; Zhao, L.D.; Kopp, N.; Schlegel, A. Brazing of ceramic-to-ceramic and ceramic-to-metal joints in air. *Front. Mech. Eng. China* **2010**, *5*, 125–129. [[CrossRef](#)]
57. Liu, G.W.; Qiao, G.J.; Wang, H.J.; Yang, J.F.; Lu, T.J. Pressureless brazing of zirconia to stainless steel with Ag-Cu filler metal and TiH₂ powder. *J. Eur. Ceram.* **2008**, *28*, 2701–2708. [[CrossRef](#)]
58. Tillmann, W.; Anar, N.B.; Wojarski, L. Mechanical behavior of reactive air brazed (RAB) Crofer 22 APU-Al₂O₃ joints at ambient temperature. *SN Appl. Sci.* **2020**, *2*, 809. [[CrossRef](#)]
59. Kuhn, B.J.; Wetzel, F.; Steinbrech, R.; Malzbender, J.; Singheiser, L. Mechanical characterization of brazed ceramic/metal joints for SOFC stacks. In Proceedings of the 8th European SOFC Forum, Lucerne, Switzerland, 30 June–4 July 2008. CD-ROM.
60. Zhou, W.L.; Hu, S.P.; Yang, M.J.; Luo, Y.; Fu, W.; Song, X.G. Reactive air brazing of 3YSZ ceramic to aluminized Crofer22H stainless steel using Ag-CuO fillers. *Int. J. Appl. Ceram. Technol.* **2022**, *19*, 2367–2378. [[CrossRef](#)]
61. Si, X.Q.; Cao, J.; Ritucci, I.; Talic, B.; Feng, J.C.; Kiebach, R. Enhancing the long-term stability of Ag based seals for solid oxide fuel/electrolysis applications by simple interconnect aluminization. *Int. J. Hydrog. Energy* **2019**, *44*, 3063–3074. [[CrossRef](#)]
62. Si, X.Q.; Wang, D.; Li, C.; Qi, J.L.; Cao, J. Exploring the role of Mn-Co spinel coating on Crofer 22 APU in adjusting reactions with the Ag based sealant during reactive air brazing. *J. Mater. Res. Technol.* **2022**, *16*, 608–618. [[CrossRef](#)]
63. Le, S.R.; Shen, Z.M.; Zhu, X.D.; Zhou, X.L.; Yan, Y.; Sun, K.N.; Zhang, N.Q.; Yuan, Y.X.; Mao, Y.C. Effective Ag-CuO sealant for planar solid oxide fuel cells. *J. Alloys Compd.* **2010**, *496*, 96–99. [[CrossRef](#)]
64. Weil, K.S.; Hardy, J.S. Development of a New Ceramic-to-Metal Brazing Technique for Oxygen Separation/Generation Applications. In Proceedings of the 2002 Fossil Energy Conference, Pittsburgh, PA, USA, 2 April 2002.
65. Chen, L.; Li, C.; Si, X.Q.; Wang, X.Y.; Wang, Z.Q.; Cao, J. A novel Ag-CuAlO₂ sealant for reactive air brazing of 3YSZ and AISI 310S. *Ceram. Int.* **2021**, *47*, 31413–31422. [[CrossRef](#)]
66. Kiebach, R.; Engelbrecht, K.; Grahl-Madsen, L.; Sieborg, B.; Chen, M.; Hjelm, J.; Norrman, K.; Chatzichristodoulou, C.; Hendriksen, P.V. An Ag based brazing system with a tunable thermal expansion for the use as sealant for solid oxide cells. *J. Power Sources* **2016**, *315*, 339–350. [[CrossRef](#)]
67. Zink, N.M.; Meier, A.M.; Weil, K.S.; Hardy, J.S. Reactive Air Brazing of LSCoF and Alumina with Ag-V₂O₅ Alloys for SOFC Applications. In *Advances in Ceramic Coatings and Ceramic-Metal Systems: Ceramic Engineering and Science Proceedings*; The American Ceramics Society: Columbus, OH, USA, 2005; pp. 341–348.
68. Sun, Z.; Zhang, L.X.; Li, X.; Zhang, S.S. Reactive air brazing of the YSZ/AISI 310s couples using a novel Ag-Nb₂O₅ sealant. *Ceram. Int.* **2020**, *46*, 5168–5174. [[CrossRef](#)]
69. Wang, Z.Q.; Li, C.; Si, X.Q.; Yang, B.; Huang, Y.X.; Qi, J.L.; Feng, J.C.; Cao, J. Brazing YSZ ceramics by a novel SiO₂ nanoparticles modified Ag filler. *Ceram. Int.* **2020**, *46*, 16493–16501. [[CrossRef](#)]

70. Barabash, V.; Federici, G.; Rödig, M.; Snead, L.L.; Wu, C.H. Neutron irradiation effects on plasma facing materials. *J. Nucl. Mater.* **2000**, *283–287*, 138–146. [[CrossRef](#)]
71. Wu, C.H.; Alessandrini, C.; Bonal, P.; Grote, H.; Moormann, R.; Rödig, M.; Roth, J.; Werle, H.; Vieider, G. Overview of EU CFCs development for plasma facing materials. *J. Nucl. Mater.* **1998**, *258–263*, 833–838. [[CrossRef](#)]
72. Barabash, V.; Akiba, M.; Mazul, I.; Ulrickson, M.; Vieider, G. Selection, development and characterisation of plasma facing materials for ITER. *J. Nucl. Mater.* **1996**, *233–237*, 718–723. [[CrossRef](#)]
73. Tanabe, T. Revisiting Carbon Materials as Plasma-Facing Materials of a Fusion Reactor. *Plasma Phys. Rep.* **2019**, *45*, 300–314. [[CrossRef](#)]
74. Ferraris, M.; Casalegno, V. Integration and joining of ceramic matrix composites. In *Ceramic Matrix Composites: Materials, Modeling and Technology*; Bansal, N.P., Lamon, J., Eds.; Wiley: Hoboken, NJ, USA, 2014; pp. 549–567.
75. Giancarli, L.; Golfier, H.; Nishio, S.; Raffray, R.; Wong, C.; Yamada, R. Progress in blanket designs using SiCf/SiC composites. *Fusion Eng. Des.* **2002**, *61–62*, 307–318. [[CrossRef](#)]
76. Iveković, A.; Novak, S.; Dražić, G.; Blagoeva, D.; de Vicente, S.G. Current status and prospects of SiCf/SiC for fusion structural applications. *J. Eur. Ceram.* **2013**, *33*, 1577–1589. [[CrossRef](#)]
77. Singh, M.; Lara-Curzio, E. Design, Fabrication, and Testing of Ceramic Joints for High Temperature SiC/SiC Composites. *ASME J. Eng. Gas Turbines Power* **2000**, *123*, 288–292. [[CrossRef](#)]
78. Riccardi, B.; Nannetti, C.A.; Woltersdorf, J.; Pippel, E.; Petrisor, T. High Temperature Brazing for SiC and SiCf/SiC Ceramic Matrix Composites. *Ceram. Trans.* **2002**, *144*, 311–322.
79. Riccardi, B.; Nannetti, C.A.; Woltersdorf, J.; Pippel, E.; Petrisor, T. Brazing of SiC and SiCf/SiC composites performed with 84Si-16Ti eutectic alloy: Microstructure and strength. *J. Mater. Sci.* **2002**, *37*, 5029–5039. [[CrossRef](#)]
80. Ahmad, I.; Silberglitt, R.; Tian, Y.L.; Katz, J.D. *Microwave Joining of SiC Ceramics and Composites*; Los Alamos National Lab (LANL): Los Alamos, NM, USA, 1997.
81. Singh, M.; Matsunaga, T.; Lin, H.-T.; Asthana, R.; Ishikawa, T. Microstructure and mechanical properties of joints in sintered SiC fiber-bonded ceramics brazed with Ag–Cu–Ti alloy. *Mater. Sci. Eng. A* **2012**, *557*, 69–76. [[CrossRef](#)]
82. Yang, J.; Zhang, X.Y.; Ma, G.L.; Lin, P.P.; Xu, Y.Q.; Lin, T.S.; He, P.; Long, W.M.; Li, J. Microstructural evolution and mechanical property of a SiCf/SiC composite/Ni-based superalloy joint brazed with an Au-Cu-Ti filler. *J. Eur. Ceram.* **2021**, *41*, 2312–2322. [[CrossRef](#)]
83. Yang, J.; Zhang, X.; Ma, G.; Lin, P.; Xu, Y.; Liu, Z.; Lin, T.; He, P.; Song, K. A study of the SiCf/SiC composite/Ni-based superalloy dissimilar joint brazed with a composite filler. *J. Mater. Res. Technol.* **2021**, *11*, 2114–2126. [[CrossRef](#)]
84. Zhang, Y.; Guo, X.M.; Guo, W.; Zhang, H.Q.; Shao, T.W.; Yu, Z.L. Effect of Cu foam on the microstructure and strength of the SiCf/SiC-GH536 brazed joint. *Ceram. Int.* **2022**, *48*, 12945–12953. [[CrossRef](#)]
85. Zhang, X.Y.; Lin, J.C.; Wang, W.; Yu, D.; Ma, G.L.; Lin, T.S.; Lin, P.P.; He, P.; Zhao, J.Q. Directly construct a gradient brazed joint of SiCf-SiC and Ni-based superalloy using a high-temperature AuCuV filler. *Mater. Sci. Eng. A* **2022**, *836*, 142722. [[CrossRef](#)]
86. Kapoor, R.R.; Eagar, T.W. Oxidation Behavior of Silver- and Copper-Based Brazing Filler Metals for Silicon Nitride/Metal Joints. *J. Am. Ceram. Soc.* **1989**, *72*, 448–454. [[CrossRef](#)]
87. Lee, D.B.; Woo, J.H.; Park, S.W. Oxidation behavior of Ag-Cu-Ti brazing alloys. *Mater. Sci. Eng. A* **1999**, *268*, 202–207. [[CrossRef](#)]
88. Anheier, N.C.; Qiao, H.; Berglin, E.J.; Hatchell, B.K. *Summary of the Preliminary Optical ICHMI Design Study: A Preliminary Engineering Design Study for a Standpipe Viewport*; Pacific Northwest National Lab (PNNL): Richland, WA, USA, 2013.
89. Prasser, H.M.; Böttger, A.; Zschau, J. A new electrode-mesh tomograph for gas–liquid flows. *Flow Meas. Instrum.* **1998**, *9*, 111–119. [[CrossRef](#)]
90. Kickhofel, J.; Yang, J.M.; Prasser, H.M. Designing a high temperature high pressure mesh sensor. *Nucl. Eng. Des.* **2018**, *336*, 122–128. [[CrossRef](#)]
91. Twentyman, M.E. High-temperature metallizing. *J. Mater. Sci.* **1975**, *10*, 765–776. [[CrossRef](#)]
92. Bao, G.; Suo, Z. Remarks on Crack-Bridging Concepts. *ASME Appl. Mech. Rev.* **1992**, *45*, 355–366. [[CrossRef](#)]
93. Feng, J.; Herrmann, M.; Reinecke, A.-M.; Hurtado, A. Interface optimization for thermal residual stress reduction at laser-brazed ceramic-stainless steel joints for miniaturized energy sensors. In Proceedings of the EuroMat 2023, Frankfurt, Germany, 3–7 September 2023.
94. Feng, J.; Herrmann, M.; Reinecke, A.-M.; Hurtado, A. Deterministic processing of alumina with nanosecond laser pulses for energy applications. In Proceedings of the EuroMat 2023, Frankfurt, Germany, 3–7 September 2023.
95. Reyes, J.N.; Groome, J.T.; Woods, B.G.; Jackson, B.; Marshall, T.D. Scaling analysis for the high temperature Gas Reactor Test Section (GRTS). *Nucl. Eng. Des.* **2010**, *240*, 397–404. [[CrossRef](#)]
96. Aoto, K.; Dufour, P.; Hongyi, Y.; Glatz, J.P.; Kim, Y.; Ashurko, Y.; Hill, R.; Uto, N. A summary of sodium-cooled fast reactor development. *Prog. Nucl. Energy* **2014**, *77*, 247–265. [[CrossRef](#)]
97. Lin, C.C. A review of corrosion product transport and radiation field buildup in boiling water reactors. *Prog. Nucl. Energy* **2009**, *51*, 207–224. [[CrossRef](#)]
98. Sandlin, S.; Kosonen, T.; Hokkanen, A.; Heikinheimo, L. Use of brazing technique for manufacturing of high temperature fibre optical temperature and displacement transducer. *Mater. Sci. Technol.* **2007**, *23*, 1249–1255. [[CrossRef](#)]
99. Schilm, J.; Goldberg, A.; Partsch, U.; Dürfeld, W.; Arndt, D.; Pönicke, A.; Michaelis, A. Joining technologies for a temperature-stable integration of a LTCC-based pressure sensor. *J. Sens. Sens. Syst.* **2016**, *5*, 73–83. [[CrossRef](#)]

100. Okamoto, N.; Miura, K.; Kondo, K.; Asano, T.; Banno, H. Brazing technology for low temperature cofired ceramics and its application to MCM. In Proceedings of the 1995 Japan International Electronic Manufacturing Technology Symposium, Omiya, Japan, 4–6 December 1995; pp. 40–43.
101. Monti, R.; Coppola, F.; Gasbarri, P.; Lecci, U. Residual stress brazing process induced in hybrid package for ISP applications. *Acta Astronaut.* **2010**, *66*, 897–913. [[CrossRef](#)]
102. Walker, C.A.; Uribe, F.; Monroe, S.L.; Stephens, J.J.; Goetze, R.S.; Hodges, V.C. High-temperature joining of low temperature cofired ceramics. In Proceedings of the 3rd International Brazing and Soldering Conference, San Antonio, TX, USA, 24–26 April 2006; pp. 54–59.
103. Ni, M.; Leung, M.K.H.; Leung, D.Y.C. Technological development of hydrogen production by solid oxide electrolyzer cell (SOEC). *Int. J. Hydrog. Energy* **2008**, *33*, 2337–2354. [[CrossRef](#)]
104. Weil, K.S.; Coyle, C.A.; Hardy, J.S.; Kim, J.Y.; Xia, G.G. Alternative planar SOFC sealing concepts. *Fuel Cells Bull.* **2004**, *2004*, 11–16. [[CrossRef](#)]
105. Kim, J.Y.; Hardy, J.S.; Weil, K.S. Silver-copper oxide based reactive air braze for joining yttria-stabilized zirconia. *J. Mater. Res.* **2005**, *20*, 636–643. [[CrossRef](#)]
106. Sun, Y.S.; Driscoll, J.C. A new hybrid power technique utilizing a direct Copper to ceramic bond. *IEEE Trans. Electron Devices* **1976**, *23*, 961–967. [[CrossRef](#)]
107. Luo, Y.; Song, X.G.; Hu, S.P.; Xu, Z.Q.; Li, Z.H.; Lei, Y. Reactive air brazing of Al₂O₃ ceramic with Ag-CuO-Pt composite fillers: Microstructure and joint properties. *J. Eur. Ceram. Soc.* **2021**, *41*, 1407–1414. [[CrossRef](#)]
108. Conze, S.; Poenicke, A.; Martin, H.P.; Rost, A.; Kinski, I.; Schilm, J.; Michaelis, A. Manufacturing Processes for TiO_x-Based Thermoelectric Modules: From Suboxide Synthesis to Module Testing. *J. Electron. Mater.* **2014**, *43*, 3765–3771. [[CrossRef](#)]
109. Martin, H.P.; Pönicke, A.; Kluge, M.; Sichert, I.; Rost, A.; Conze, S.; Wätzig, K.; Schilm, J.; Michaelis, A. TiO_x-Based Thermoelectric Modules: Manufacturing, Properties, and Operational Behavior. *J. Electron. Mater.* **2016**, *45*, 1570–1575. [[CrossRef](#)]
110. Börner, F.D.; Schreier, M.; Feng, B.; Lippmann, W.; Martin, H.P.; Michaelis, A.; Hurtado, A. Development of laser-based joining technology for the fabrication of ceramic thermoelectric modules. *J. Mater. Res.* **2014**, *29*, 1771–1780. [[CrossRef](#)]
111. Feng, B.; Martin, H.-P.; Börner, F.-D.; Lippmann, W.; Schreier, M.; Vogel, K.; Lenk, A.; Veremchuk, I.; Dannowski, M.; Richter, C.; et al. Manufacture and Testing of Thermoelectric Modules Consisting of B_xC and TiO_x Elements. *Adv. Eng. Mater.* **2014**, *16*, 1252–1263. [[CrossRef](#)]
112. Mukerjee, S.; Leah, R.; Selby, M.; Stevenson, G.; Brandon, N.P. Chapter 9—Life and Reliability of Solid Oxide Fuel Cell-Based Products: A Review. In *Solid Oxide Fuel Cell Lifetime and Reliability*; Brandon, N.P., Ruiz-Trejo, E., Boldrin, P., Eds.; Academic Press: Cambridge, MA, USA, 2017; pp. 173–191.
113. Woïrgard, E.; Arabi, F.; Sabbah, W.; Martineau, D.; Theolier, L.; Azzopardi, S. Identification and analysis of power substrates degradations subjected to severe aging tests. *Microelectron. Reliab.* **2015**, *55*, 1961–1965. [[CrossRef](#)]
114. Kiebach, W.R.; Knibbe, R.; Frederiksen, K.B.; Chen, M.; Mikkelsen, L.; Hendriksen, P.V. Investigation of Failure Mechanisms in Ti Containing Brazing Alloys Used in SOFC/SOEC Environments. In Proceedings of the ASME 2010 8th International Conference on Fuel Cell Science, Engineering and Technology, Brooklyn, NY, USA, 14–16 June 2010; pp. 655–665.
115. Qiao, G.J.; Zhang, C.G.; Jin, Z.H. Thermal cyclic test of alumina/kovar joint brazed by Ni-Ti active filler. *Ceram. Int.* **2003**, *29*, 7–11. [[CrossRef](#)]
116. Dandapat, N.; Ghosh, S.; Pal, K.S.; Datta, S.; Guha, B.K. Thermal cycling behavior of alumina-graphite brazed joints in electron tube applications. *Trans. Nonferrous Met. Soc. China* **2014**, *24*, 1666–1673. [[CrossRef](#)]

Disclaimer/Publisher’s Note: The statements, opinions and data contained in all publications are solely those of the individual author(s) and contributor(s) and not of MDPI and/or the editor(s). MDPI and/or the editor(s) disclaim responsibility for any injury to people or property resulting from any ideas, methods, instructions or products referred to in the content.